PRESERVATION OF NICOTINE AND SOLANESOL FROM TOBACCO BY CYCLODEXTRINS NANOENCAPSULATION

BY

MR. SORRAWEE CHULURKS

A THESIS SUBMITTED IN PARTIAL FULFILLMENT OF THE REQUIREMENTS FOR THE DEGREE OF MASTER OF SCIENCE (ENGINEERING AND TECHNOLOGY) SIRINDHORN INTERNATIONAL INSTITUTE OF TECHNOLOGY THAMMASAT UNIVERSITY ACADEMIC YEAR 2020 COPYRIGHT OF THAMMASAT UNIVERSITY

PRESERVATION OF NICOTINE AND SOLANESOL FROM TOBACCO BY CYCLODEXTRINS NANOENCAPSULATION

BY

MR. SORRAWEE CHULURKS

A THESIS SUBMITTED IN PARTIAL FULFILLMENT OF THE
REQUIREMENTS FOR THE DEGREE OF MASTER OF
SCIENCE (ENGINEERING AND TECHNOLOGY)
SIRINDHORN INTERNATIONAL INSTITUTE OF TECHNOLOGY
THAMMASAT UNIVERSITY
ACADEMIC YEAR 2020
COPYRIGHT OF THAMMASAT UNIVERSITY

THAMMASAT UNIVERSITY
SIRINDHORN INTERNATIONAL INSTITUTE OF TECHNOLOGY

THESIS
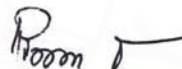
BY

MR. SORRAWEE CHULURKS

ENTITLED

PRESERVATION OF NICOTINE AND SOLANESOL FROM TOBACCO BY CYCLODEXTRINS NANOENCAPSULATION

was approved as partial fulfilment of the requirements for the degree of Master of Science (Engineering and Technology)
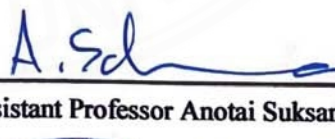
on 16 June, 2021

Chairperson

(Associate Professor Pisanu Toochinda, Ph.D.)

Member and Advisor

(Associate Professor Luckhana Lawtrakul, Dr.rer.nat.)

Member

(Colonel Assistant Professor Anotai Suksangpanomrung, Ph.D.)

Director

(Professor Pruettha Nanakorn, D.Eng.)

Thesis Title	PRESERVATION OF NICOTINE AND SOLANESOL FROM TOBACCO BY CYCLODEXTRINS NANOENCAPSULATION
Author	Mr. Sorrawee Chulurks
Degree	Master of Science (Engineering and Technology)
Faculty/University	Sirindhorn International Institute of Technology/ Thammasat University
Thesis Advisor	Associate Professor Luckhana Lawtrakul, Dr.rer.nat.
Academic Years	2020

ABSTRACT

Tobacco wastes contain major valuable active compounds which are nicotine and solanesol. Nicotine is widely used in pharmaceutical industries, especially for smoking cessation. There are several products for nicotine replacement therapy such as chewing gum, lozenges, and patches. Solanesol has many bioactivities such as antioxidant, anti-inflammatory, neuroprotective, and antimicrobial which can be used for pharmaceutical products. However, nicotine and solanesol instability caused by volatile substances, heat, presence of sunlight, or oxidizing agents, limits their usage. Therefore, the preservation of both active compounds is needed. The nanoencapsulation by using β-cyclodextrin (βCD) and methylated-β-cyclodextrin (MβCD) were investigated due to their non-toxicity. Computer simulation was used to predict the possibility of nicotine/CDs and solanesol/CDs inclusion complexes formation. The computer simulation results show the 1:1 and 2:1 host-guest molar ratio for nicotine/CDs and solanesol/CDs, respectively, which were further verified by experimental study. XRD, FTIR, TGA, and DSC results were analyzed to confirm the inclusion complexes formation. The preservation study of nicotine was performed at 25 °C and 40 °C for 21 days. The remaining amount of pure nicotine are 51.20% and 50.34% for 25 °C and 40 °C, respectively. Nicotine/βCD and nicotine/MβCD

inclusion complexes show the stability improvement of nicotine. The remaining amount of nicotine from nicotine/βCD and nicotine/MβCD inclusion complexes are 85.84% and 82.72% for 25 °C and 89.32% and 76.22% for 40 °C, respectively. The preservation study of solanesol was performed at 25 °C and 40 °C for 28 days. The remaining amount of pure solanesol are 63.13% and 54.27% for 25 °C and 40 °C, respectively. Solanesol/βCD and solanesol/MβCD inclusion complexes show the stability improvement of solanesol. The remaining amount of solanesol from solanesol/βCD and solanesol/MβCD inclusion complexes are 96.91% and 96.77% for 25 °C and 94.59% and 87.34% for 40 °C, respectively. The results show that the nanoencapsulation technique using cyclodextrins can be performed to enhance the stability of both nicotine and solanesol when compared to the free forms which results in the shelf-life extension of nicotine and solanesol. Moreover, a skin permeation study shows the increment of permeated nicotine after being encapsulated by CDs. After 60 min, nicotine/βCD gel provides highest amount of permeated nicotine which is 13.57 μg followed by nicotine/MβCD gel, 9.81 μg, and pure nicotine gel, 0.95 μg. The improvement of nicotine skin permeation result can be applied for further use in the pharmaceutical industries.

ACKNOWLEDGEMENTS

Mr. Sorrawee Chulurks

TABLE OF CONTENTS

LIST OF TABLES

LIST OF FIGURES

LIST OF SYMBOLS/ABBREVIATIONS

Symbols/Abbreviation	Terms
°C	Degree Celsius
Å	Angstrom
αCD	Alpha-Cyclodextrin
βCD	Beta-Cyclodextrin
γCD	Gamma-Cyclodextrin
ATR	Attenuated Total Reflection
CD	Cyclodextrin
DSC	Differential Scanning Calorimetry
DTG	Differential Thermal Gravimetric
FDA	Food and Drug Administration
FTIR	Fourier-Transform Infrared Spectroscopy
GC-FID	Gas Chromatography-Flame Ionization Detector
h	Hour
HPLC	High Performance Liquid Chromatography
KBr	Potassium Bromide
MβCD	Methylated-Beta-Cyclodextrin
mM	Millimolar
mL	Milliliters
OSHA	Occupational Safety and Health Administration
PM	Physical Mixture
rpm	Revolution per Minute
s	Second
TG	Thermal Gravimetric
TGA	Thermogravimetric Analysis
XRD	X-ray Diffractometry

CHAPTER 1

INTRODUCTION

1.1 Introduction

Tobacco (*Nicotiana spp., L.*) is a plant of the Solanaceae family and the general term for many products prepared from tobacco leaves. More than 70 species of tobacco are known, but the chief commercial crop is *N.tabacum* (Jadhav, Kengar, Nikam, & Bhutkar, 2019). Normally, dried tobacco leaves are mainly used for smoking in cigarette; however, tobacco wastes from the cigarette production contain the active compounds which are nicotine and solanesol (Jokić, Gagić, Knez, Banožić, & Škerget, 2019). Nicotine, an alkaloid compound, is widely used in pharmaceutical industry for nicotine replacement therapy for smoking cessation in form of pills, lozenges, and patches. Moreover, nicotine also has antimicrobial and insecticidal activities (McIndoo, 1916; Tucker & Pretty, 2005). However, nicotine is an unstable substance due to highly volatile and hygroscopic properties. The preservation of nicotine is needed to extend the shelf life of nicotine contained products.

Solanesol is a trisesquiterpenoid alcohol (Hudsin, 2015; Yan et al., 2015) with all trans stereoisomers. Solanesol is widely used as a pharmaceutical intermediate of ubiquinone coenzyme Q10 and vitamin K2 synthesis (Tang et al., 2007; Tucker & Pretty, 2005; Yan et al., 2019). Moreover, solanesol has several bioactivities such as antioxidant, anti-inflammatory, neuroprotective, and antimicrobial activities. However, solanesol is easy to decompose when exposed to air. Therefore, the preservation of solanesol is needed.

A nanoencapsulation technique is widely used in several industries such as textile industries, food industries, and pharmaceutical industries. Since nicotine and solanesol, as a guest molecule, are used in pharmaceutical industrial, the host molecule for the encapsulation must be a non-toxic substance. β-cyclodextrin (βCD) and methylated-β-cyclodextrin (MβCD), derivative of βCD, were selected due to their non-toxicity approved by Food and Drug Administration (FDA) (Ezhilarasi, Karthik, Chhanwal, Anandharamakrishnan, & Technology, 2013; Szente & Szejtli, 1999). βCD is a cyclic oligomer composed of 7 glucose molecules, in a cylinder-shaped

structure with hydrophilic outer surface and hydrophobic inner cavity (Del Valle, 2004; Pinho, Grootveld, Soares, & Henriques, 2014). According to the structure, βCD has the ability to form the inclusion complex with the active compounds by the encapsulation process. The inclusion complex can protect the encapsulated guest molecule from temperature, heat, light, volatility, and any undesired reactions. However, βCD has low aqueous solubility (KLEPTOSE®) which might affect the encapsulation efficiency. MβCD was introduced as an alternative host molecule. The presence of methyl groups in MβCD leads to the enhancement of aqueous solubility and may improve the encapsulation efficiency of inclusion complexes. The host-guest molar ratio for preparing nicotine/CDs and solanesol/CDs inclusion complexes were suggested by the results of computer simulation.

Moreover, skin permeation of nicotine/CDs inclusion complex was investigated due to the general nicotine contained product in pharmaceutical application which is transdermal patches. Transdermal patch composed of 3 components: backing layer, matrix, and release liner. Generally, the active compound is added to the matrix part of the patch. Therefore, to compare the nicotine skin permeation, pure nicotine and nicotine in the form of inclusion complexes were added into gel matrices. These gel matrices were used in the skin permeation study. The skin permeation study was performed using Franz's cell diffusion with pig skin as a medium.

Therefore, this work focused on the preservation of two active compounds, nicotine and solanesol, by nanoencapsulation technique using βCD and MβCD. The complex formations of nicotine and solanesol with βCD and MβCD were verified by FTIR, XRD, DSC, and TGA characterization techniques. The encapsulation efficiencies and preservation capabilities of the inclusion complexes were evaluated and compared to those of the pure compounds. Moreover, skin permeation study of nicotine in form of the inclusion complexes were evaluated and compared to the pure compound.

1.2 Statement of Problem

Active compounds from plants are usually unstable. They can decompose, alter their forms, or react with other compounds especially in particular environment. The presence of heat, sunlight, oxidizing agents, or exposure to high temperature accelerates those processes. Decomposed or degraded active compounds cannot provide their activities as usual. The reduction of activities or the presence of adverse activities may develop (Yan et al., 2019). Those problems lead to commercially impractical use of several active compounds (Coimbra et al., 2011). To maintain their activities, the storing condition must be taken into careful consideration. Low shelf life and difficulty in the quality control process of the active compound contained products are also obvious.

In this study, problems of active compounds, including nicotine and solanesol, were investigated. Nicotine is easy to evaporate and oxidize. Normally, nicotine is used as the treatment of nicotine dependence to eliminate smoking and the damage to human health. The controlled amount of nicotine is provided in form of gums, dermal patches, lozenges, inhalers, or electronic cigarettes for patients to quit from smoking. However, by storing of nicotine at room temperature and opening to atmosphere, nicotine is rapidly degraded. In case that nicotine can be encapsulated, the shelf life will be extended. Solanesol is the key for synthesis ubiquinone drug (coenzyme Q10 and vitamin K2). However, solanesol is easy to oxidize (Ezhilarasi, Karthik, Chhanwal, & Anandharamakrishnan, 2013) with atmosphere. Therefore, nanoencapsulation by using cyclodextrins is a promising technique to preserve as well as maintain the activities of nicotine and solanesol.

1.3 Objectives of the study

     1.3.1 To investigate the inclusion complex formation between active compounds, nicotine and solanesol, and CDs

     1.3.2 To investigate preservation efficiency of nicotine/CDs and solanesol/CDs inclusion complexes and compared to pure compounds.

     1.3.3 To investigate skin permeation of nicotine in the form of inclusion complexes compared to nicotine in free form.

1.4 Scope of the study

This study focused on the preservation of active compounds, nicotine and solanesol by nanoencapsulation technique. The nanoencapsulation host are βCD and MβCD and guests are nicotine and solanesol. The preservation studies of nicotine and solanesol in the form of inclusion complex were performed. Moreover, the skin permeation study of nicotine/CDs inclusion complex was performed based on the pharmaceutical application of nicotine.

CHAPTER 2
LITERATURE REVIEW

2.1 Active tobacco compounds from tobacco waste

In cigarette making industrial, there are many tobacco wastes left over from the process. However, tobacco wastes contain several active compounds that can be used in many applications such as pharmaceutical application, food industrial, and used as insecticidal application. The major active compounds in tobacco wastes are nicotine and solanesol. There are several studies about nicotine and solanesol extraction process. However, nicotine and solanesol have low stability due to air, temperature, and sunlight (short shelf life). Therefore, nanoencapsulation technique was interested in this study.

2.1.1 Nicotine

Nicotine is an alkaloid compound composed of pyrrolidine and pyridine rings that normally found in tobacco leaves (Balandrin, Klocke, Wurtele, & Bollinger, 1985; de Ong, 1924). The major form of nicotine in natural is in S-(-) isomer (Figure 2.1) while R-(+) isomer (Figure 2.2) is found in small amount. However, R-(+) isomer can be increased from 0.1%-11% due to pyrolytic racemization from smoking. The properties of nicotine have been shown in Table 2.1. Amount of nicotine contained in dry tobacco is around 2-7 µg/kg. However, nicotine content can be varied due to many factors such as tobacco strains, cultivated conditions, and tobacco curing.
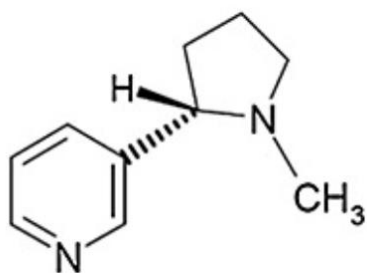
Figure 2.1 Structure of (R)-Nicotine
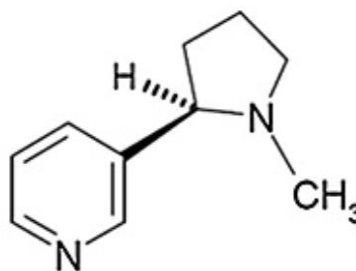
Figure 2.2 Structure of (S)-Nicotine

There are 3 major strains of tobacco that are normally used in Thailand which are Turkish, Burley, and Virginia. Turkish strain tobacco has a strong flavor from the essential oils due to sun-cured process. Burley strain tobacco is an air-cured tobacco with several properties such as good combustion and high absorption of flavor additives. Virginia strain tobacco is a flue-cured tobacco that present most in cigarette (40-70%). The amounts of nicotine and others compounds in different tobacco strains are shown in Table 2.2.

Table 2.1 Properties of nicotine

Property	Description
IUPAC name	3- [(2S)-1-methylpyrrolidin-2-yl] pyridine
CAS no.	54-11-5
Molecular weight	162.236 g/mol
Melting point	-79 °C
Boiling point	247 °C (1 atm)
Density	1.01 g/cm^3 at 25 °C
Soluble	Soluble in ethanol (50 mg/mL)
Storage condition	Keep under inert gas, hygroscopic, air and light sensitive

(Sources: www.sigmaaldrich.com and pubchem.ncbi.nlm.gov)

Table 2.2 Amounts of nicotine and others compounds in tobacco

Strains	Nicotine content (%)	Sugar content (%)	Ash content (%)	pH
Turkish	1.04	13.96	11.82	4.83
Burley	3.13	0.50	19.00	5.48
Virginia	2.30	18.75	12.00	5.10

(Source: PubChem database and Sigma-Aldrich Co. LLC.)

2.1.1.1 Application of nicotine

Nicotine is used in several applications. The primary using of nicotine is use for nicotine dependence treatment to eliminate smoking and the health damages. The controlled amounts of nicotine are provided in form of gums, dermal patches, lozenges, inhalers, or electronic cigarettes to help patients for quitting from smoking. In addition, nicotine can be used to recover the patients' health conditions from dementia and schizophrenia, dopaminergic neurons and axons, and also used to decrease the intake of harmful substances for smokers in nicotine aided smoking cessation (Tayoub, Sulaiman, & Alorfi, 2015). Some evidence verify that nicotine can reduce some symptoms of Parkinson's, Alzheimer's, and severe depression. Nicotine possesses antioxidant property, anti-microbial property (Tucker & Pretty, 2005). Moreover, nicotine is also use as insecticidal due to its insecticidal activities (McIndoo, 1916).

2.1.1.2 Toxicity of nicotine

Nicotine is very toxic to human and animals. According to Occupational Safety and Health Administration or OSHA, nicotine is categorized as an extremely deadly substance. An exposure route is by ingestion, inhalation, and skin absorption. The legal limit set by OSHA for nicotine in workplace is 0.5 mg/m^3 for skin exposure over an 8 hours workday (Hudsin, 2015). At environmental levels of 5 mg/m^3, nicotine is immediately dangerous to life and health. The exposure to nicotine in human can lead to nausea, vomiting, headache, diarrhea, and respiratory failure.

2.1.1.3 Stability of nicotine

Using nicotine as insecticide, which is used in both direct contact and fumigating modes (Krake, 1999). A fumigant is any kinds of pesticides that is active under its gaseous state. Nicotine, which is a volatile alkaloid, can be vaporized to gas easily under a normal condition. From volatilization test, the free form of nicotine was found to be quickly volatile (de Ong, 1924). The free form of nicotine is also very hygroscopic, i.e., readily to absorb moisture, and can undergo oxidation easily in the presence of air, heat, or light. The oxidation involves a free radical reaction (Gorrod & Jacob III, 1999); however, no detail study is performed. The identified degradation products are cotinine, methylamine, myosmine, and nicotine-N-l'-oxide (Wada, Kisaki, & Saito, 1959). The level of nicotine degraded after exposure to high temperatures with the presence of air at 1 atm may increase up to 8% as shown in Table 2.3 (Hadaruga, Hadaruga, Butnaru, Tatu, & Gruia, 2010).

Table 2.3 Amount of remaining nicotine after exposure to temperature and air

| T (°C) | Remaining nicotine (%) | |
	2 h	6 h
30	95.9%	95.7%
90	93.7%	92.6%

(Sources: Hădărugă, Hădărugă, Butnaru, Tatu, & Gruia, 2010)

2.1.1.4 Nicotine extractions

Nicotine is a high value substance that can be extracted from tobacco leaves or tobacco wastes. Extraction process can be performed by several techniques including Soxhlet extraction, ultrasonic assisted extraction, microwave assisted extraction, supercritical fluid extraction, and column-chromatography extraction (CCE) (Hu et al., 2015a; Ng & Hupé, 2003). From literature review, supercritical fluid provides the high yield of nicotine (Ruiz-Rodriguez, Bronze, & da Ponte, 2008). However, the developed methods of nicotine extraction such as microwave assisted and supercritical fluid extraction require the specific instruments and large amount of solvent. Since industrial scale extraction requires low cost, the developed methods are not proper for nicotine extraction.

2.1.2 Solanesol

Solanesol (Figure 2.3) is a trisesquiterpenoid alcohol (Hudsin, 2015; Yan et al., 2015) with all trans stereoisomers. Solanesol is accumulated in solanaceous plants such as tobacco, potato, and tomato (Hudsin, 2015; Yan et al., 2015). Solanesol is highest accumulation in tobacco when compared to solanaceous plants. All solanesol in nature are trans stereoisomer. At room temperature, pure solanesol is in form of a waxy white solid. Solanesol is completely insoluble in water but slightly soluble in methanol and ethanol. It is miscible in hexane, chloroform, and acetone due to the non-polar or weakly polar property. The properties of solanesol are provided in Table 2.4.

Table 2.4 Properties of solanesol

Property	Description
IUPAC name	(2E,6E,10E,14E,18E,22E,26E,30E)-3,7,11,15,19,23,27,31,35-nonamethylhexatriaconta-2,6,10,14,18,22,26,30,34-nonaen-1-ol
CAS no.	13190-97-1
Molecular weight	631.1 g/mol
Melting point	33-35 °C
Boiling point	685.6°C (1atm)
Density	0.889 g/cm^3 at 25 °C
Soluble	Insoluble in water (0.00031 g/L) but soluble in organic solvent
Storage condition	Keep under -20 °C
Molecular size (approx. from PM6)	38.291 Å × 6.199 Å × 6.275 Å

(Sources: Sources: www.sigmaaldrich.com and pubchem.ncbi.nlm.gov)
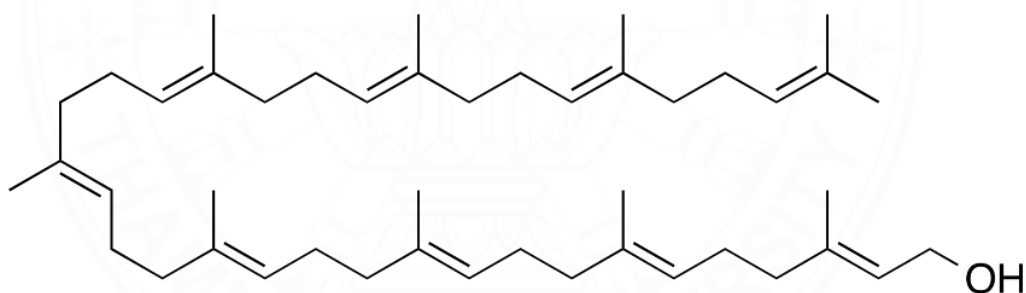
Figure 2.3 Structure of solanesol

2.1.2.1 Application of solanesol

Solanesol possesses several bioactivities such as antioxidant, anti-inflammatory activity, neuroprotective activity, and antimicrobial activities. Solanesol has strong antioxidant activity because there are several non-conjugated double bonds. Huang et al. studied about solanesol extraction from tobacco leaves by using supercritical CO_2. Huang et al. found that solanesol crude that extracted from tobacco leaves exhibited good anti-free radical activity (Huang, Li, Niu, Wang, & Qin, 2008). Anti-inflammatory activity of solanesol was studied against carrageenan-induces hind paw oedema. Furthermore, solanesol herbal gel can be used as topical anti-inflammatory products (P. Sridevi, P. Vijayanand, & M. B. Raju, 2017). The derivative of solanesol is also used for treating acquired immune deficiency syndrome (AIDS) and wound healing (Tang et al., 2007; Yan et al., 2015).

Moreover, solanesol is used as a pharmaceutical intermediate for the ubiquinone drugs synthetic (e.g., coenzyme Q10 and Vitamin K) and also anticancer agent synergizer SDB (Tang et al., 2007; Tucker & Pretty, 2005; Yan et al., 2019). Coenzyme Q10 participates in mitochondrial respiratory chain and ATP synthesis. Coenzyme Q10 was used for treating patients with neurodegenerative disease, hypertension, and cardiovascular disease and can be used as dietary supplements for diabetes patients. Moreover, coenzyme Q10 has many functions such as antioxidant activity, enhancement of immune, and regulate the blood lipid. Vitamin K2, a lipid-soluble vitamin, has effect in prevention and treatment of osteoporosis. Furthermore, solanesol can be used for enhancing tumor suppression effect and reducing toxicity of anticancer drugs. The new diacid solanesyl 5-fluororacil ester derivatives with effective antitumor activity and low toxicity was synthesized by Xiao et al. (Xiao Keyi, 2012).

2.1.2.2 Toxicity of solanesol

Solanesol is a non-volatile particulate phase in cigarette smoke (Armitage, Dixon, Frost, Mariner, & Sinclair, 2004). The cigarette smoking contains several sub-micron particles from incomplete combustion of cigarette which inhaled into respiratory track and lung. Chemicals carried by particles from smoking lead to various diseases such as chronic obstructive pulmonary and lung cancer (Cui, Yurteri, Cabot, Xie, & Liu, 2019). Nowadays, there is no study confirms about toxicity of solanesol or LD_{50} of solanesol in human. However, United State Patent Document provided toxicity of solanesol toward mouse. The result shown that LD_{50} from intraperitoneal route is more than 4,000 mg/kg.

2.1.2.3 Stability of solanesol

Solanesol is easy decompose when expose to air because oxygen in air can be reacted with solanesol (oxidation reaction) as shown in Figure 2.4 (Tucker & Pretty, 2005). Samuel P. Tucker found out that there are three products from solanesol that can be generated by ozonation are isoprenoid acetone, ω-hydroxy isoprenoid acetaldehydes and isoprenoid oxoaldehydes. His study also determined the amount of solanesol loss when exposed to ambient air compared to ozone from ozone generator which shown in Figure 2.5 below.

Moreover, Samuel P. Tucker also investigated the stability of solanesol during storage process. He found out that solanesol in methanol solution with tightly sealed in florescence room at room temperature has shelf-life about 3.6 month. However, average recovery of solanesol in solid state was only 11% after 6 days at room temperature, in the dark (Tucker & Pretty, 2005).
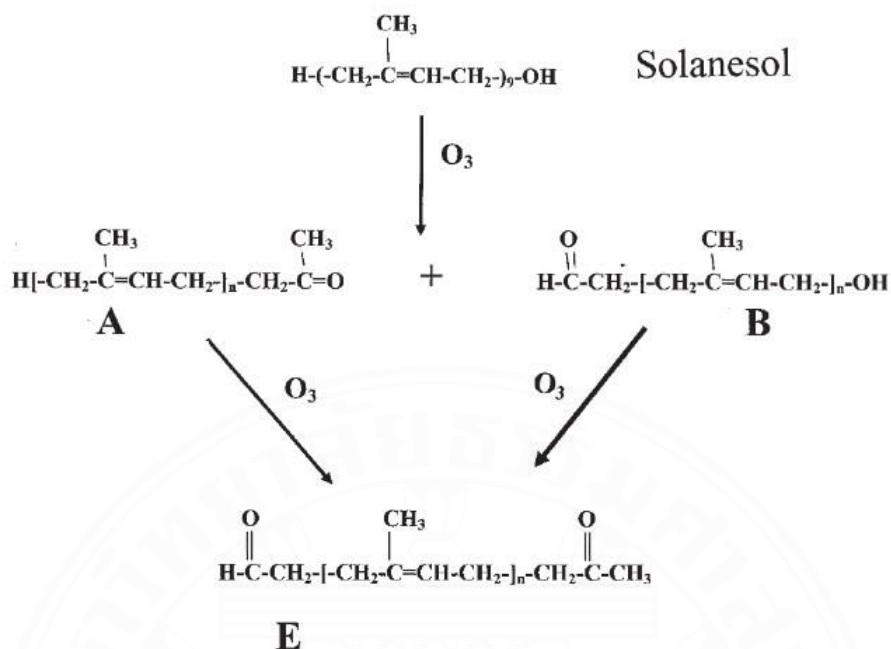
Figure 2.4 Products from solanesol ozonation: A) isoprenoid acetone, B) ω-hydroxy
isoprenoid acetaldehydes and C) isoprenoid oxoaldehydes
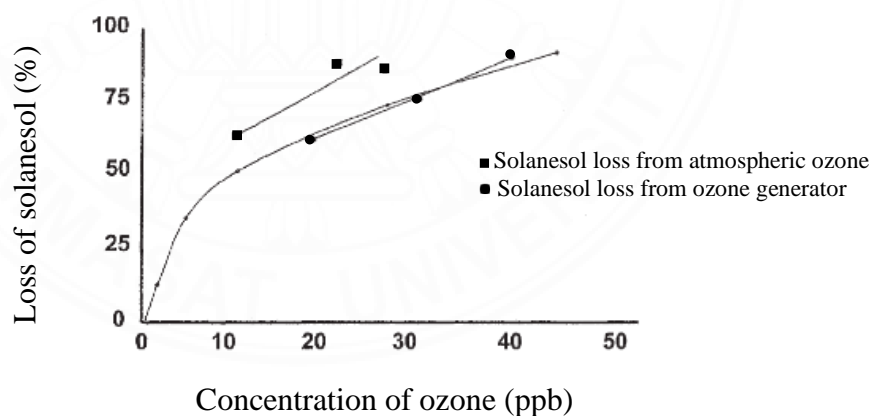
Figure 2.5 Loss of solanesol in different conditions

2.1.2.4 Extraction of Solanesol

Solanesol accumulation in each part of plants is different. Hu et al. investigated the amounts of solanesol in different parts of tobacco including leaves, stalk, stems, and roots. The results revealed that the highest solanesol content is from the leaves which is 0.45%. Moreover, Liu et al found that different points of tobacco leaves contain different amount of solanesol. The highest solanesol content is at upper leaf and then middle leaf, and lower leaf, respectively (Liu XP, 2007). Solanesol extraction can be performed by several methods. Table 2.5 shown methods that can be used. There are 2 factors that affect the solanesol content in plants which are genetic and environment. For genetic factor, solanesol content are different in 93 tobacco germplasms by range of variety is 1.78-3.60% of dry matter (Yan et al., 2015). Xiang et al. studied the amount of solanesol in different planting geographical regions of Chinese flue-cured tobacco germplasms and found that the percentage of solanesol content in flue-cured tobacco were ranged from 0.70-4.13% (Xiang et al., 2017).

For environmental factor, Ning Yan found that when tobacco exposed to moderate high temperatures (30°C for daytime and 24°C for nighttime) resulted in significant increase of solanesol accumulated as shown in Figure 2.6. The reason of increasing solanesol accumulation after exposure to moderate high temperature is tobacco increased geranylgeranyl diphosphate synthase, 1-deoxy-d-xylulose 5-phosphate reductoisomerase, N. tabacum 3-hydroxy-3-methylglutaryl-CoA reductase, and solanesyl diphosphate synthase genes (Yan et al., 2018).

Table 2.5 Solanesol extraction methods

Extraction methods	Description	References
Ammonia Leaching Pretreatment Assisted Extraction	• Hexane was used a solvent for solanesol extraction • Purpose of this method is enhanced effectiveness of solanesol extraction • Extraction yield is increased from 89.24% to 104.63% and the purity is increased from 16.72% to 21.03%	(Sun et al., 2013; ZHAO, YANG, ZU, XIA, & XIAO, 2007)
Dynamic Saponification Extraction	• Naphtha solvent and ethanol were used for solanesol extraction via saponification • Mass ratio of NaOH in 80% ethanol (v/v) to tobacco crude extract is 1:4 • Dynamic saponification treatment can be increased the extraction yield by 9.30% when compared to conventional saponification	(ZHAO et al., 2007)
Ultrasonic Assisted Extraction	• Use acetone as solvent for extract solanesol from tobacco leaves • Ratio of wastes to solvent is 1:17.5 (g/mL) at temperature 60 °C • Yield of product is 94.70%	(Zhang & Feng, 2007)

Table 2.6 Solanesol extraction methods (cont.)

Extraction methods	Description	References
Supercritical Fluid Extraction	• Required low extraction temperature • Using supercritical CO_2, pressure is 20 MPa, at 55 °C, for 90 minutes, and 95% of ethanol was used • then subjected solanesol crude from extraction to silica gel column • petroleum ether: ether: ethyl acetate: acetone (15:5:3:1 by volume) for separation and elution • mass fraction of solanesol product is greater than 98%	(MI, 2005; Wang & Gu, 2018)
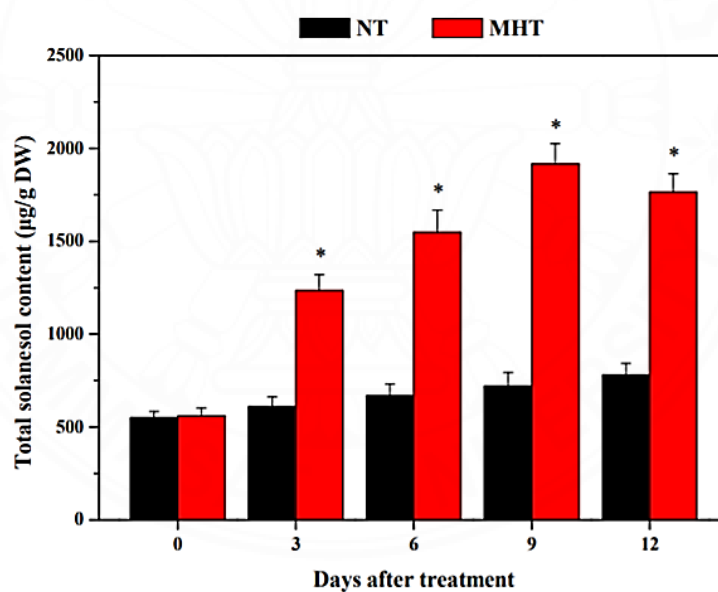
Figure 2.6 Amount of solanesol content in tobacco leaves compared between NT (normal temperature) and MHT (moderate high temperature)

2.2 Cyclodextrin

Cyclodextrin (CD) is a cyclic glucose molecule derived from a starch degradation by enzyme that produced from *Bacillus* genus (Pinho et al., 2014) called Cyclodextrin glucanotransferase (CGTase). CGTase enzyme cleaves two end of linear polysaccharide and link them together to make a cyclic ring of CD. Shape of CD is a truncated cone shape with hydrophobic inner cavity from a carbon ether skeleton and hydrophilic outer surface from hydroxyl groups. Due to its molecular structure, CD is able to form inclusion complex with several compounds (Del Valle, 2004). CDs have been widely applied in the pharmaceutical, food, cosmetic, textile industries, and in analytical. Some promising applications of CD used in industries are stabilization of light-sensitive and volatile compounds, masking of odor and flavor in food industries, increasing the solubility of drug, drug delivery, and selective extraction.

2.2.1 Structural of cyclodextrin

Cyclodextrin is composed of glucose linked together via α-1, 4-glucopyranose bond and results in the conformation as shown in Figure 2.7 (Astray, Gonzalez-Barreiro, Mejuto, Rial-Otero, & Simal-Gandara, 2009). An inner cavity is lined by the carbon ether skeleton (glycosidic oxygen bridges) and hydrogen atoms (at the position 3 and 5). Secondary hydroxyl groups (at the position 2 and 3) line on the outer wider edge of the ring, while primary hydroxyl group (at the position 6) lines on another edge. The molecular alignment gives CD hydrophilic surface and hydrophobic cavity as shown in Figure 2.8.
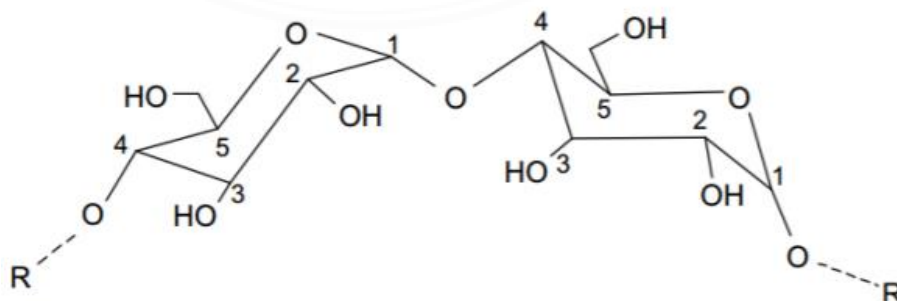
Figure 2.7 α-1,4-glucopyranose bond (Astray, Gonzalez-Barreiro et al. 2009)
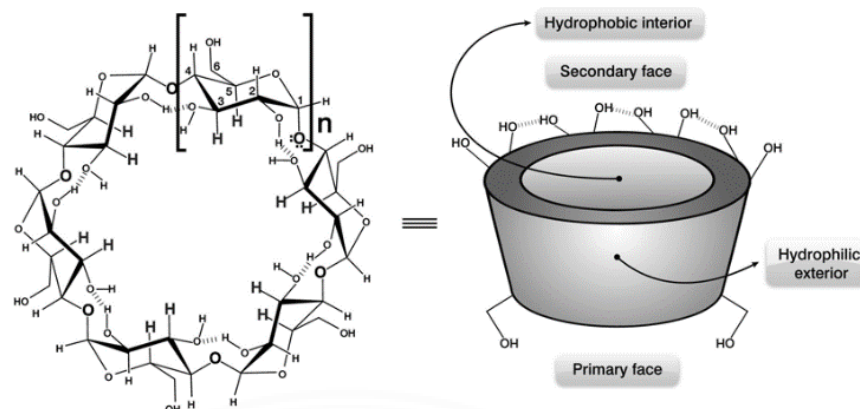
Figure 2.8 Structure of CD and hydrophilic and hydrophobic locations (Linde, Laverde, & Colauto, 2011)

2.2.2 Classification of conventional cyclodextrin

The number of glucose units comprised to be CD molecule is the key to classify CDs. CD is naturally present in three forms, separated by number of glucose molecules including αCD with glucose molecules, βCD with 7 glucose molecules, and γCD with 8 glucose molecules (Pinho et al., 2014). The differences in the number of glucose units result in the differences of physical and chemical properties of CDs, including their molecular weights, solubilities, polarities, and cavity sizes as shown in Table 2.7. The suitability of CDs depends on the compound that was encapsulated inside their cavities. Among 3 conventional CDs, βCD is the widely used one in the commercial products because of its lowest price and suitability towards many compounds. Moreover, these three conventional CDs were approved by FDA in many countries such as USA, Canada, Japan, Korea, and Thailand (Ezhilarasi, Karthik, Chhanwal, & Anandharamakrishnan, 2013; Szente & Szejtli, 1999).

Table 2.7 Properties of αCD, βCD, and γCD [a] (Singh, Bharti, Madan, & Hiremath, 2010), b *(Szejtli, 2004)*

Properties	α-cyclodextrin	β-cyclodextrin	γ-cyclodextrin
No. of glucose units[a]	6	7	8
Molecular weight[a]	972	1135	1297
Aqueous solubility at 25 °C (mg/mL)[b]	129.5	18.4	249.2
Cavity diameter (Å)[b]	4.7-5.3	6.0-6.5	7.5-8.3
Height of torus (Å)[b]	7.9 ± 0.1	7.9 ± 0.1	7.9 ± 0.1
Outer diameter (Å)[b]	14.6 ± 0.4	15.4 ± 0.4	17.5 ± 0.4
Volume of cavity (Å^3)[b]	174	262	427
Volume of cavity (mL/mol)[b]	0.10	0.14	0.20
Price of Food Grade CD (USD/kg)[a]	45.0	5.0	80.0
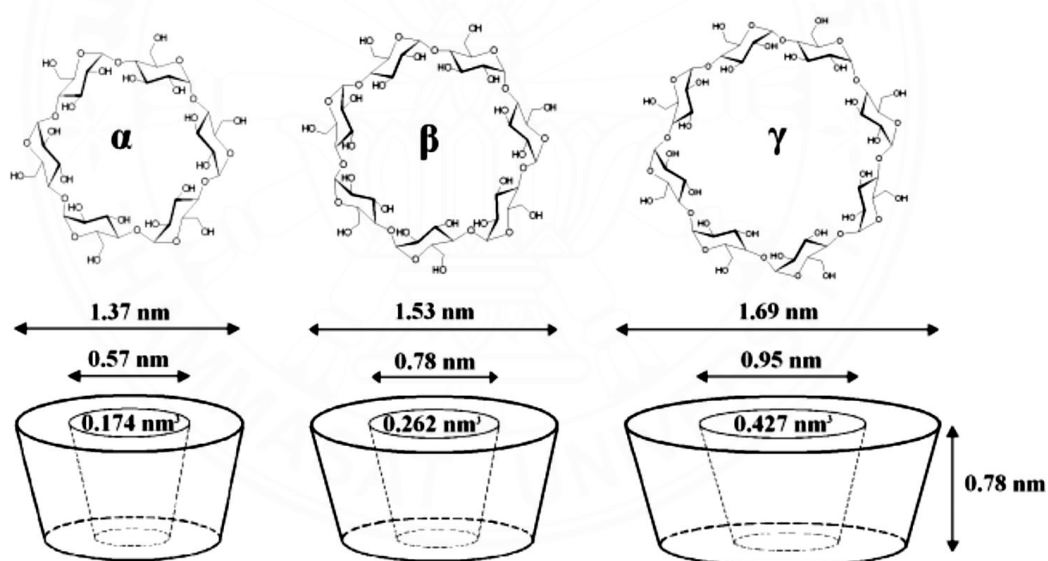
Figure 2.9 Structures of αCD, βCD, and γCD (Jin, 2013)

Between three conventional CDs, βCD is the one that commonly use due to the price and suitability when compared to αCD and γCD. However, the main problem of βCD is low aqueous phase solubility compared to others. The way to increase the solubility of βCD is heating or dissolve in mixture of suitable co-solvent such as ethanol. Figure 2.10 shows the solubility of βCD in different conditions (different of mixture and temperature). Solubility of βCD was increased significantly as temperature increases. The addition of ethanol into mixture also increases the βCD solubility, maximum concentration of ethanol that can make βCD reaches highest solubility is 30 vol% in aqueous solution. Table 2.8 shown the solubility of βCD in different organic solvent and mixture of solvents in water.
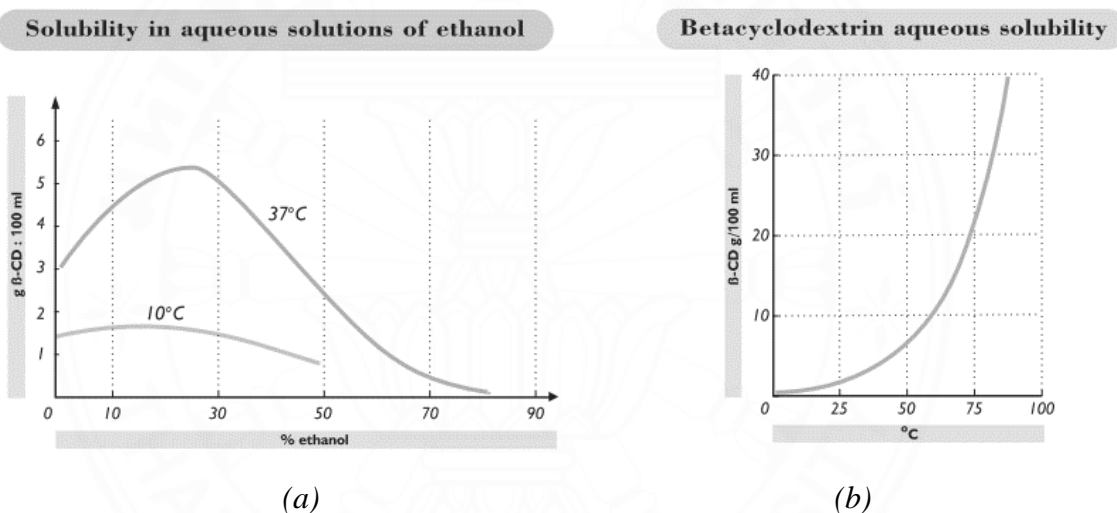
Figure 2.10 (a) Solubility of βCD in ethanol-water solution and (b) solubility of βCD as function of temperature (Source: www.roquette.com)

Table 2.8 Solubility of βCD in various solvents of mixtures

Solvent	Pure solvent		Mixture (50% solvent:50% water)	
	25 °C	45 °C	25 °C	45 °C
Methanol	Insoluble	Insoluble	Insoluble	<1
Ethanol	Insoluble	Insoluble	<1	3
Isopropanol	Insoluble	Insoluble	>1	8
Ethylene glycol	21	33	1	2
Propylene glycol	2	10	5	5
Glycerin	Insoluble	Insoluble	Insoluble	Insoluble

Note: solubility is in a unit of g of βCD/100 mL (source: www.roquette.com)

2.2.3 Derivative of cyclodextrin

Since CD has low aqueous phase solubility, lead to limitation of preparation techniques. Therefore, CD derivative was introduced due to their higher aqueous phase solubility. Derivative form of CD was produced from 2 ways which are chemical modification and enzymatic modification (Szente & Szejtli, 1999). The process to modify CD is to substitute primary (location 1 and 2) and secondary hydroxyl groups (location 6) of CD as shown in Figure 2.11. The substituents of hydroxyl groups change the properties of derivatives, compared to natural CDs. Some modified properties are solubility, stability, cavity volume, and ability to bind or release the guest molecule (Jin, 2013). Table 2.9 show properties of derivative of CD and their chemical structure. However, cost of derivative CD quite high due to their properties and modification process. Normally, there are 5 forms of derivative CD that use in industrial which are methylated derivative of βCD, hydroxylpropylated βCD, sulfobutylated-βCD, branched CDs, and acetylated βCD and γCD (Hirayama & Uekama, 1999; Szente & Szejtli, 1999)
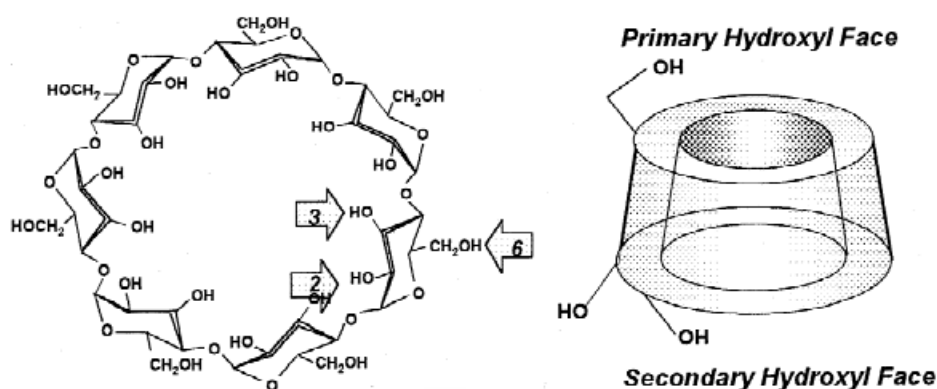
Figure 2.11 Chemical structure of CD with possible substituent locations

(Source: Hirayama & Uekama, 1997)

Table 2.9 Properties, prices, and uses of some CD derivatives

CD derivatives	Molecular formula	Aqueous solubility at 25 °C (mg/mL)	Price USD/g	Uses
Dimethyl-βCD	$C_{56}H_{98}O_{35}$	> 500	74.2	Similar to βCD
Trimethyl-βCD	$C_{63}H_{112}O_{35}$	312.5	160.0	Similar to βCD
2-Hydroxypropylated-βCD	$C_{63}H_{12}O_{42}$	> 500	14.3	Similar to βCD, Parenteral formulation

(Source: www.sigmaaldrich.com)

2.2.4 Inclusion complex formation

Cyclodextrin acting as a capsule to provide a space for active compounds, called host molecule. Active compounds, nicotine and solanesol, called as guest molecules. Normally, any guest molecules that have molecule size fit with inner cavity of host molecule can form inclusion complex. For CDs inclusion complex formation, inner cavity of CD is hydrophobic. Therefore, the possibility to form inclusion complex between CD and hydrophobic guest molecule will be higher than normally (Astray et al., 2009). The inclusion complex formation is the substitution if included water molecule in the cavity of CD by guest molecule. Formation process of inclusion complex are as follows:

1. CD's inner cavity release the water molecule lead to formation of a more favorable hydrophilic and hydrophilic interaction with bulk water content in solution (Astray et al., 2009).

2. After water released, guest molecule wans included inside CD's cavity and forms a more favorable hydrophobic and hydrophobic interaction lead to high stability state (Astray et al., 2009).

3. Interaction between host and guest are hydrophobic interaction, van der Waals, and hydrogen bonds.

4. The release of steric strain of CD as the complex is formed.

Moreover, not only water but also co-solvent and non-aqueous solvent can use in the formation of an inclusion complex (Astray et al., 2009). Type of interactions between host and guest molecules are non-covalent interaction such as van der Waals force, hydrogen bonds, and other hydrophobic interactions.
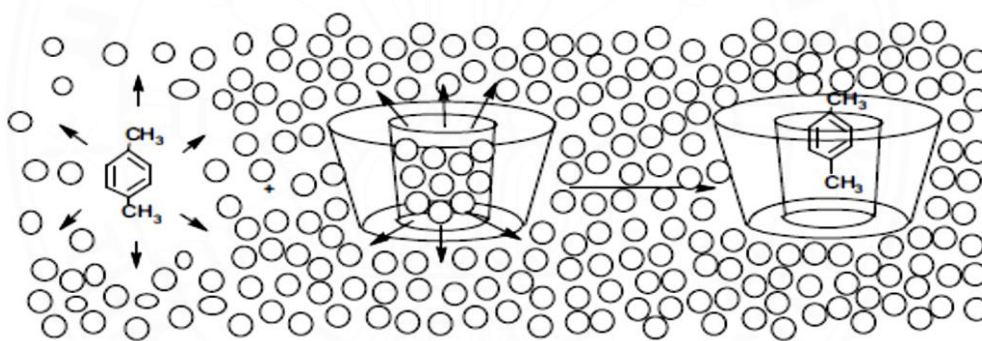
Figure 2.12 Formation of inclusion complex (Astray et al., 2009)

In example, Figure 2.12 shows the inclusion complex formation of guest which is xylene. Xylene has high hydrophobic energy due to a repulsive interaction with hydrophilic solvent molecules. The CD's hydrophobic cavity is also high energy state due to repulsive interaction with hydrophilic solvent molecules. After the formation of inclusion complex was formed, xylene was substituted water molecule inside CD's cavity and get included inside. Total energy of system decreases because of favorable interaction between xylene and CD's cavity and expelled water molecule and bulk water molecule in solution (Astray et al., 2009).

2.2.5 Preparation of inclusion complex

Inclusion complex can be prepared in both solution and solid state. The advantage of solid-state preparation is less expensive, but sometime yields low inclusion complex formation efficiency. Commonly, preparation of inclusion complex in solution is used industry. However, inclusion complex in form of inclusion complex is prone to be more difficult to store and handle. Therefore, another process that needed is recovery process. Table 2.10 shows the example of the inclusion complex preparations and recovery techniques by drying of CD.

Table 2.10 Examples of inclusion complex preparation methods

Method	Description
Physical mixing	Physical mixture of CD and guest is prepared and physical blended. This method is not effective as the mixing time can be ranged from hour to days (Del Valle, 2004; Hedges, 1998)
Co-precipitation	This method is widely use in laboratory. CD is dissolved in solution and guest is added while stirring. The condition is selected to collect an inclusion complex as precipitation. CD solution can be heated up to high temperature. After guest molecule is added; the solution is cooled down to precipitate the complex. However, the scale-up is difficult as it requires large amount of water or solvent (Del Valle, 2004; Hedges, 1998).
Co-mixing and Drying	CD and guest molecules are prepared in the solution. The solution was mixed and stirred for certain period. The formed complex can be recovered by drying (Del Valle, 2004).

CHAPTER 3
METHODOLOGY

In this work, the preservation of nicotine and solanesol were studied by the nanoencapsulation technique using βCD and MβCD. The methodology of this work was separated into two sections, which are nanoencapsulation of nicotine and solanesol as follows. Moreover, skin permeation of nicotine in the form of inclusion complexes was conducted and compared to pure nicotine.

3.1 Nanoencapsulation of nicotine
3.1.1 Computational simulation method

The x-ray crystal structure of nicotine, β-cyclodextrin (βCD), and 2,6-O-methyl-β-cyclodextrin (MβCD) were downloaded from the Cambridge crystallographic Data Centre with identifier: YOCZUM (Jiang, Tang, & Lu, 2008), BCDEXD03 (Steiner & Koellner, 1994), and BOYFOK03 (Manunza, Deiana, Pintore, & Gessa, 1997), respectively. The modification of atoms and bonds were done via Discovery Studio 4.0 Visualizer(Biovia, 2017) then minimized by density functional theory M06-2X using basis set 6-31G(d,p) calculations via Gaussian16 program package (Frisch et al., 2016). Optimized nicotine was then docked into the cavity of both βCD and MβCD molecules via AutoDock 4.2 (Morris et al., 2009). The βCD and MβCD molecules (hosts) were kept rigid, while nicotine molecule (guest) was allowed to move freely inside the host's cavity. One hundred docking calculations were performed on each host-guest complex using the Lamarckian genetic algorithm with remaining parameters run at default settings (Morris et al., 2009). The results obtained were classified into different clusters with different molecular docking binding energy. The docked conformation with the lowest energy in each cluster was selected to be the representative for further minimization using M06-2X/6-31G(d,p) method. The complexation energy (ΔE) of 1:1 molecular ratio between nicotine/βCD and nicotine/MβCD in the minimized geometries were evaluated by Equation. (3.1).

$$\Delta E = E_{complex}^{Opt} - (E_{host}^{Opt} + E_{guest}^{Opt}) \tag{3.1}$$

where $E_{complex}^{Opt}$, E_{host}^{Opt} and E_{guest}^{Opt} represented to the minimization energy of the host-guest inclusion complex, host molecule (either βCD or MβCD) and guest molecule (nicotine), respectively.

3.1.2 Materials for nicotine encapsulation

(S)-nicotine (99%, Alfa Aesar, Massachusetts, USA) was used as the guest molecule for nanoencapsulation and the standard for calibration curve. βCD (98.0%, Tokyo Chemical Industry, Japan) and MβCD (Mixture of several methylated, Tokyo Chemical Industry, Japan) were used as host molecules for nicotine. For nicotine/CD inclusion complex characterization, absolute ethanol (HPLC grade, RCI Labscan Thailand) was used as a solvent to prepare nicotine standard solution for GC-FID and to extract nicotine from the inclusion complex. Nicotine gels were prepared for skin permeation study. Carbopol gel was prepared by using carbopol 940 dissolve with ethanol (AR grade, RCI Labscan Thailand) and propylene glycol (Laboratory reagent, KEMAUS Australia). Phosphate buffer solution, methanol (AR grade, RCI Labscan Thailand) and triethylamine (Laboratory reagent, KEMAUS Australia) were used as the mobile phases to determine the amount of permeated nicotine through pig skin by HPLC.

3.1.3 Preparation and evaluation of nicotine inclusion complex

3.1.3.1 Solvent effect on inclusion complex preparation

Generally, ethanol is introduced as a co-solvent in inclusion complex preparation method to improve the solubility of βCD. Therefore, the optimum concentration of ethanol needs to be investigated. 181.6 and 215.1 mg of βCD and MβCD, respectively was prepared in solutions by dissolving in 10 mL of 0, 5, and 10 vol% of ethanol-water solutions. Nicotine was added into each CD solution at equivalent amount to 1:1 molar ratio between host (βCD and MβCD) and guest (nicotine) as the suggestion from computational simulation. Then the solid inclusion complex was recovered from the solutions by the freeze-drying method and determined encapsulation efficiency by GC-FID. The appropriate concentration was found at a 0 vol% of ethanol-water solution which was used to prepare the nicotine inclusion complex in this study.

Encapsulated nicotine was extracted from solid complexes by dissolving solid complexes with ethanol and sonicating at 40 °C for 45 min. The extracted nicotine was filtered by using syringe filter 0.22 μm before analyzed with GC-FID. The encapsulation efficiency of the complex formation was determined using the Equation (3.2).

$$\text{Encapsulation efficiency} = \frac{\text{Amount of nicotine encapsulated}}{\text{Amount of nicotine initially added}} \times 100 \qquad (3.2)$$

3.1.3.2 Effect of recovery methods on inclusion complex preparation

To obtain solid inclusion complexes, the recovery method is needed. In this study, two recovery methods were studied which are freeze-drying and oven drying methods. Freeze-drying is a recovery method for heat sensitive active compound due to low operating temperature to obtain solid complex; however, freeze-drying method required high cost for operating and maintenance. Therefore, oven drying method was introduced as an alternative for recovery method with lower operating and maintenance cost. Oven drying method is the recovery method using hot air to obtain solid complex. The temperature was set to be lower than active compound's boiling point.

In this study, recovery method of nicotine inclusion complexes was performed by both oven drying and freeze-drying to compare encapsulation efficiency. For oven drying, solutions were dried by oven at 60 °C for 72 h. For freeze-drying, solutions were dried by using freeze dryer (Model: Freeze Dryer -55 °C, Operon, Gyeonggi-do, Korea). Nicotine solid complexes from both recovery methods were stored at 4 °C before determining the encapsulated efficiency by GC-FID. The encapsulation efficiency of the inclusion complexes was determined using the Equation (3.2).

3.1.3.3 Preparation of nicotine/βCD and nicotine/MβCD inclusion complex

Nicotine inclusion complexes were prepared by dissolve 545.4 mg of βCD and 628.8 mg of MβCD in 30 mL of water. Solutions were shaking in shaker for 3 h and added nicotine into each solution at equivalent amount to 1:1 molar ratio between host and guest. The inclusion complex solutions were shaking in incubator shaker at 25 °C for 72 h. Recovered solid complex by using oven dry for 72 h and stored at 4 °C before use. Figure 3.1 illustrates nicotine/CDs inclusion complex obtained from freeze-drying and oven drying methods.

Figure 3.1 Nicotine/CDs inclusion complex obtained from freeze-drying and oven drying methods (from left to right)

3.1.4 Characterization

3.1.4.1 Gas chromatography-flame ionization detector (GC-FID)

The amount of nicotine in the complex was determined by using GC-FID (Clarus 580, Perkin Elmer, Massachusetts, USA coupled with a HP-5 ((5%-phenyl)-methylpolysiloxane, 30 m length × 0.25 mm I.D. × 0.25 μm film column, Agilent, USA) as shown in Figure 3.2. The injection volume was set to 1 μL with a split ratio of 10:1. The injection temperature was set to 260 ℃. Carrier gas that was helium with a flow rate of 2 mL/min. The temperature program was set to 120 ℃ and hold for 2 min and then ramped to 250 ℃ at a rate of 15 ℃/min and hold for 2 min. The detector temperature was set at 260 ℃ and the range of detector was set to 1 with an attenuation of 5.

Figure 3.2 Clarus 580 GC-FID

3.1.4.2 High performance liquid chromatography (HPLC)

The amount of permeated nicotine from nicotine/CDs inclusion complexes through pig skin was determined by HPLC (1260 Infinity II LC system, Agilent Technologies, California, USA) equipped with a G7111A quaternary pump, a G7129A vial sampler, a G7116A multicolumn thermostat, and a G7114A variable wavelength detector as shown in Figure 3.3. The separation of analyte was performed with C18 column (Luna 5 μm C18(2) 100 Å, 250 mm × 4.6 mm column, Phenomenex, California, USA) with the controlled column temperature of 25 °C. Phosphate buffer solution (0.08 M and pH 6.5), methanol, and triethylamine were used as mobile phase in the ratio of 55.8:40:4.2 at flow rate 1 mL/min. HPLC sample was prepared and filtered by 0.22 μm syringe filter before injection. The injection volume was set at 20 μL and the separated analytes were detected by UV detector at 260 nm for 20 minutes.

Figure 3.3 1260 Infinity II LC system HPLC

3.1.4.3 Fourier transform infrared spectroscopy (FTIR)

The FTIR spectrograms of, nicotine, CDs, and inclusion complexes were characterized by using a FTIR spectrometer (Nicolet iS50, Thermo Fisher Scientific, Massachusetts, USA) as shown in Figure 3.4. FTIR solid samples were prepared by mixed between 1% (w/w) of sample and spectral grade KBr (Specac, Pennsylvania, USA) and grounded into powder. The obtained powder was pressed into a thin disk using a hydraulic press at 1 ton for 60 s. The spectrograms of each sample were recorded at wavenumbers between 400 and 4000 cm^{-1} with 16 scans and a resolution of 4 cm^{-1}. The FTIR spectrograms of solid samples, i.e., CDs and inclusion complex, were characterized using the transmission mode using KBr as a background. The FTIR spectrogram pure liquid nicotine was characterized using the attenuated total reflection (ATR) mode.

Figure 3.4 Nicolet iS50 FTIR spectrometer

3.1.4.4 X-ray diffractometry (XRD)

The crystalline patterns of nicotine/βCD inclusion complex and nicotine/MβCD inclusion complex were characterized by using an XRD (D8 Advance Model, Bruker, United Kingdom) to investigate the inclusion complex formation, compared to the physical mixtures. XRD was operated at a voltage of 40 kV and a current of 45 mA and a temperature of 25 °C. The crystalline patterns were recorded between 3° and 40° (2θ) with 0.02° step size and 0.5 s step time. The XRD instrument was shown in Figure 3.5.

Figure 3.5 D8 Advance Model XRD

3.1.4.5 Differential scanning calorimetry (DSC)

The energy change of inclusion complexes and pure compounds were determined by DSC 3+ (Mettler-Toledo, Columbus, OH, USA). Samples were weighed and placed in aluminum crucibles. The samples were heated from 30 °C to 300 °C at 10 °C/min under N_2 atmosphere with 50 mL/min flow rate. The DSC instrument was shown in Figure 3.6.

Figure 3.6 Mettler-Toledo DSC 3+

3.1.4.6 Thermogravimetric analysis (TGA)

Thermal analysis of inclusion complexes and pure compounds were recorded by TGA/DSC 1 (Mettler-Toledo, Columbus, OH, USA). Samples were weighed and placed in alumina crucibles. The samples were heated from 30 °C to 500 °C at 10 °C/min under N_2 atmosphere with 50 mL/min flow rate. The TGA instrument was shown in Figure 3.6.

Figure 3.7 Mettler-Toledo TGA/DSC 1

3.1.5 Evaluation of nicotine preservation efficiency

Nicotine/βCD, nicotine/MβCD inclusion complexes and pure nicotine were stored in an incubator at 25 °C and 40 °C for 21 days to evaluate the nicotine stability of both forms. Each sample was weighed 15 mg or equivalent amount of nicotine present in the complex. The evaluation was performed in triplicate. The remaining nicotine after exposure duration was extracted and its amount was determined by GC-FID. Amount of remaining nicotine was determined by Equation (3.3).

$$\%\text{Remaining nicotine} = \frac{\text{Amount of nicotine remained}}{\text{Amount of nicotine encapsulated}} \times 100 \qquad (3.3)$$

3.1.6 Determination of skin permeation rate toward pig skin

Nicotine contained pharmaceutical products are mainly used for smoking cessation treatment. One of nicotine contained products is transdermal patches. Transdermal patch can be separated to 3 parts which are backing layer, gel or matrix, and release liner. Generally, nicotine is involved in matrix part of the patches. Therefore, gel of nicotine inclusion complexes and pure nicotine were prepared for study the skin permeation toward pig skin.

3.1.6.1 Gel preparation

2.2 g of carbopol 940 was dissolved in 60 vol% of ethanol and stirred for 10 min at 800 rpm. The solution was left in room temperature at least 10 h to form a gel. 1 g of nicotine/βCD and nicotine/MβCD solid inclusion complexes were weighed separately and suspended in 2.5 mL of water. The suspended solution and 15 g of gel were mixed and left for overnight. Nicotine/CDs inclusion complex gels were stored at 4 °C before use. Figure 3.8 shows the gel products for skin permeation study.

Figure 3.8 Gels (Carbopol 940 gel, nicotine/βCD gel, and nicotine/MβCD gel from left to right)

3.1.6.2 Skin permeation study

Franz's diffusion cell (Logan Instrumental Corp., Model FDC-6, USA), as shown in Figure 3.9, was used to study nicotine skin permeation with pig skin as media. Pig skin was mounted between two half-cells of Franz's diffusion cell with dermis facing the receptor half-cell. Gel was spread on the stratum corneum surface and receptor was filled with phosphate buffer solution (PBS), pH 7.4. The PBS was removed periodically and the concentration of nicotine in PBS was determined by HPLC. The model of Franz's diffusion cell was illustrated in Figure 3.10.

Figure 3.9 Logan Instrumental Franz's diffusion cell
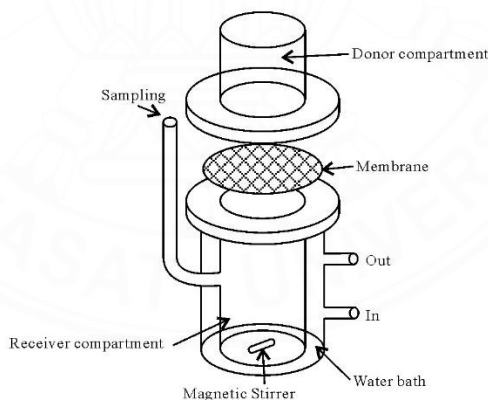
Figure 3.10 Franz's diffusion cell model

3.2 Solanesol

3.2.1 Materials for solanesol encapsulation

Solanesol (Tokyo Chemical Industrial, Japan), βCD (98.0%, Tokyo Chemical Industry, Japan), and MβCD (Mixture of several methylated, Tokyo Chemical Industry, Japan) were used for solanesol/cyclodextrin inclusion complexes preparation. Absolute ethanol (HPLC grade, RCI Labscan, Thailand) was used as a solvent to prepare solanesol standard solution for HPLC and to extract solanesol from the inclusion complexes. Acetonitrile (HPLC grade, RCI Labscan, Thailand) and isopropanol (HPLC grade, RCI Labscan, Thailand) were used as mobile phase for HPLC.

3.2.2 Preparation and evaluation of solanesol inclusion complex

3.2.2.1 Effect of ethanol on inclusion complex preparation

Since solanesol is immiscible in water, various concentrations of ethanol were concerned to optimize the inclusion complex preparation method. 363.2 mg of βCD and 419.2 mg of MβCD (equivalent to 16 mM) were dissolved in 20 mL of various concentrations of ethanol (0-90 vol%). As the computational simulation suggested, solanesol was added in each CD solution at 2:1 molar ratio and shaken in shaker at 25 °C for 72 h. To obtain solid complexes, inclusion complex solutions were dried in oven at 60 °C for 72 h and solid complexes were stored in 4 °C before use.

Encapsulated solanesol was extracted from solid complexes by dissolving solid complexes with ethanol and sonicating at 40 °C for 45 min. The extracted solanesol was filtered by using syringe filter 0.22 μm before analyzed with HPLC. The encapsulated solanesol in solid complexes were determined by HPLC and calculated by Equation (3.4). The highest encapsulation efficiency obtained from using 70 vol% ethanol-water solution.

$$\text{Encapsulation efficiency} = \frac{\text{Amount of solanesol encapsulated}}{\text{Amount of solanesol initially added}} \times 100 \qquad (3.4)$$

3.2.2.2 Preparation of solanesol/βCD and solanesol/MβCD inclusion complex

363.2 mg βCD and 419.2 mg of MβCD were dissolved in 20 mL of 70 vol% ethanol-water solution. 101 mg of solanesol was dissolved in CD solution and shaken in shaker at 25 °C for 72 h. To obtain solid complexes, inclusion complex solutions were dried in oven at 60 °C for 72 h and stored in 4 °C before use.

3.2.3 Characterization

3.2.3.1 High performance liquid chromatography (HPLC)

The amount of solanesol was determined by using HPLC (1260 Infinity II LC system, Agilent Technologies, California, USA) equipped with a G7111A quaternary pump, a G7129A vial sampler, a G7116A multicolumn thermostat, and a G7114A variable wavelength detector. The separation of analyte was performed with C18 column (Luna 5 μm C18(2) 100 Å, 250 mm × 4.6 mm column, Phenomenex, California, USA) with the controlled column temperature of 25 °C. An isocratic elution was performed by using mixture of acetonitrile and isopropanol (60:40 vol%) as mobile phase. HPLC samples were prepared and filtered by 0.22 μm syringe filter before injection. The injection volume was set at 10 μL and the separated analytes were detected by UV detector at 215 nm for 16 minutes.

3.2.3.2 Fourier transform infrared spectroscopy (FTIR)

The FTIR spectrograms of solanesol, CDs, and inclusion complex were characterized by using a FTIR spectrometer (Nicolet iS50, Thermo Fisher Scientific, Massachusetts, USA). FTIR solid samples were prepared by mixed between 1% (w/w) of sample and spectral grade KBr (Specac, Pennsylvania, USA) and grounded into powder. The obtained powder was pressed into a thin disk using a hydraulic press at 1 ton for 60 s. The spectrogram of each sample was recorded at wavenumbers between 400 and 4000 cm^{-1} with 16 scans and a resolution of 4 cm^{-1}. The FTIR spectrograms of solid samples were characterized using the transmission mode using KBr as a background

3.2.3.3 X-ray diffractometry (XRD)

The crystalline patterns of both solanesol/βCD and solanesol/MβCD inclusion complexes were characterized by using an XRD (D8 Advance Model, Bruker, United Kingdom) to investigate the inclusion complex formation, compared to pure compounds. XRD was operated at a voltage of 40 kV and a current of 45 mA and a temperature of 25 °C. The crystalline patterns were recorded between 3° and 40° (2θ) with 0.02° step size and 0.5 s step time.

3.2.3.4 Differential scanning calorimeter (DSC)

The energy change of inclusion complexes and pure compounds were determined by DSC 3+ (Mettler-Toledo, Columbus, OH, USA). Samples were weighed and placed in aluminum crucibles. The samples were heated from 30 °C to 300 °C at 10 °C/min under N_2 atmosphere with 50 mL/min flow rate.

3.2.3.5 Thermogravimetric analysis (TGA)

Thermal analysis of inclusion complexes and pure compounds were recorded by TGA/DSC 1 (Mettler-Toledo, Columbus, OH, USA). Samples were weighed and placed in alumina crucibles. The samples were heated from 30 °C to 500 °C at 10 °C/min under N_2 atmosphere with 50 mL/min flow rate.

3.2.4 Evaluation of solanesol preservation efficiency

Solanesol/βCD, solanesol/MβCD inclusion complexes, and pure solanesol were stored in an incubator and exposed to air at 25 °C and 40 °C for 28 days to evaluate the solanesol stability of both forms. Each sample was weighed 15 mg or equivalent amount of solanesol present in the complex. The evaluation was performed in triplicate. The remaining solanesol after exposure duration was extracted and its amount was determined by HPLC. Amount of remaining solanesol was determined by Equation (3.5).

$$\%\text{Remaining solanesol} = \frac{\text{Amount of solanesol remained}}{\text{Amount of solanesol encapsulated}} \times 100 \qquad (3.5)$$

CHAPTER 4

RESULTS AND DISCUSSIONS

4.1 Nicotine inclusion complex

4.1.1 Computational Simulation of nicotine/CDs inclusion complex

Computational simulation was used to predict the conformations of the inclusion complexes. Two possibility modes of nicotine orientation inside the cavity of cyclodextrins are shown in Figure 4.1. In orientation A, the pyridine ring of nicotine is located near the wide rim of the host molecule while in orientation B, the pyrrolidine moiety of nicotine is located near the wide rim of the host molecule.

Figure 4.1 Schematic illustration of possible conformations of inclusion complex

The complexation energy and the optimized inclusion complex conformations which obtained from M06-2X calculations are presented in Table 4.1 and Figure 4.2, respectively.

All negative values of complexation energy (ΔE) indicate that nicotine can form the stable 1:1 inclusion complex molecular ratio to βCD and MβCD both in orientation A and B. It has been shown that nicotine is trapped deep-down inside the cavity and binds considerable stronger to βCD than MβCD in the same orientation with magnitude of 7.1 and 3.40 kcal/mol in orientation A and B, respectively (as shown in Figure.4.2 and Table 4.1). In nicotine/βCD orientation A, one H-bond with a distance of 2.08 Å occurs between nitrogen atom of pyridine ring and hydrogen atom of the secondary hydroxyl group at O2 of βCD. No intermolecular H-bond found in nicotine/βCD orientation B and nicotine/MβCD complexes in both orientations.

Table 4.1 The calculated complexation energy ΔE, in kcal/mol, of nicotine inclusion complex with βCD and MβCD.

	Orientation A	Orientation B
nicotine/βCD	-24.51	-26.13
nicotine/MβCD	-17.41	-22.73

Some of the methyl tails at C6 positions of MβCD are enter to the cavity of itself, as depicted in Figure 4.2(c) and (d). This prevents the entry of nicotine molecule to go deep-down inside MβCD's cavity which results in the alignment of guest molecule located at the wider rim of MβCD. Methyl substitution at the secondary hydroxyl group of O2 for all seven glucose units increases the number of hydrocarbon atoms which enhances the hydrophobic interaction between host and guest molecules, especially in orientation B (Figure 4.2(d)). The theoretical study on inclusion complexes by computer simulation was used as the preliminary results to the experimental study preparation in laboratory scale.
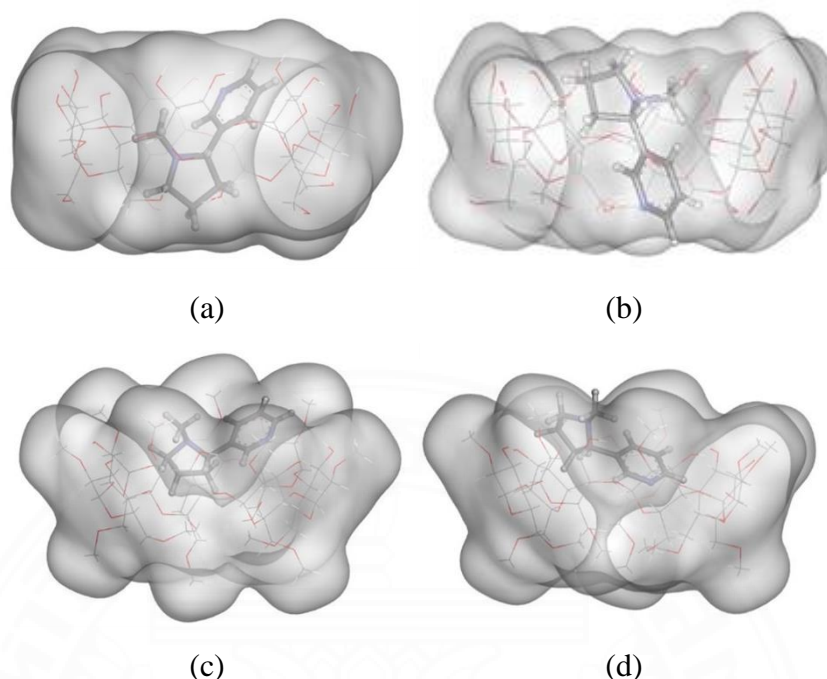
Figure 4.2 The minimized inclusion complex conformations: (a) nicotine/βCD in orientation A, (b) nicotine/βCD in orientation B, (c) nicotine/MβCD in orientation A, and (d) nicotine/MβCD in orientation B.

4.1.2 Effect of ethanol on inclusion complex preparation

Table 4.2 shown encapsulation efficiencies of nicotine inclusion complexes at various concentrations of ethanol (0-10 vol%). Results show that the increment of ethanol decreased the encapsulation efficiency. Preparation with pure water (0 vol% of ethanol) gives highest encapsulation efficiency which are 59.96 ± 1.62% and 63.76 ± 0.24% for nicotine/βCD and nicotine/MβCD, respectively. Ethanol was introduced as co-solvent for inclusion complex preparation; however, the increasing concentration of ethanol makes nicotine prefer to stay in free form. Therefore, in this study, preparation of nicotine/CDs inclusion complex was performed with pure water.

Table 4.2 Encapsulation efficiency of nicotine by freeze-drying method

Inclusion complex	Concentration of ethanol (vol%)	Encapsulation efficiency (%)
	0	76.59 ± 3.56
Nicotine/βCD	5	64.27 ± 1.58
	10	59.91 ± 2.55
	0	81.86 ± 3.14
Nicotine/MβCD	5	78.19 ± 3.92
	10	77.58 ± 0.67

4.1.3 Effect of recovery methods on inclusion complex preparation

Table 4.3 Encapsulation efficiency of nicotine by two recovery methods

Inclusion complex	Encapsulation efficiency (%)	
	Oven drying	Freeze-drying
Nicotine/βCD	59.96 ± 1.62	76.59 ± 3.56
Nicotine/MβCD	63.76 ± 0.24	81.86 ± 3.14

Table 4.3 shows the encapsulation efficiency of nicotine by two recovery methods, oven drying and freeze-drying. The recovered solid inclusion complexes from freeze-drying method have higher encapsulation efficiency due to the operating temperature. However, the inclusion complex recovery method in the industrial scale must concern about the production cost. Based on literature review, Flink was studied and compared the operating and maintenance cost between freeze-drying and oven drying method. The results revealed the 4-8 times lower cost of oven drying than freeze-drying method (Flink, 1977). Hence, the oven drying method was chosen to be conducted in this study.

4.1.4 Characterization

4.1.4.1 X-ray diffractometry (XRD)

Figure 4.3(a) shows the crystalline pattern of βCD, physical mixture and nicotine/βCD inclusion complex. Due to the liquid form of nicotine, pure nicotine cannot be characterized by this technique. Therefore, physical mixture which is the mixing between pure nicotine and βCD by kneading method was introduced for comparing between βCD and inclusion complex. Figure4.3(b) shows the crystalline pattern of MβCD. Result shows that MβCD has an amorphous crystalline pattern. Therefore, this technique cannot characterize nicotine/MβCD inclusion complex.

The characteristic peaks of βCD are at 10.73°, 12.43°, 15.39°,19.47°, 20.81°, and 22.73° (2θ). The XRD pattern of the physical mixture combines the characteristic peaks of both nicotine and βCD. However, the XRD pattern of the complex shows a different pattern comparing to patterns of physical mixture and βCD. The results indicate the difference in the crystallinity of the nicotine/βCD inclusion complex when compared to physical mixture.
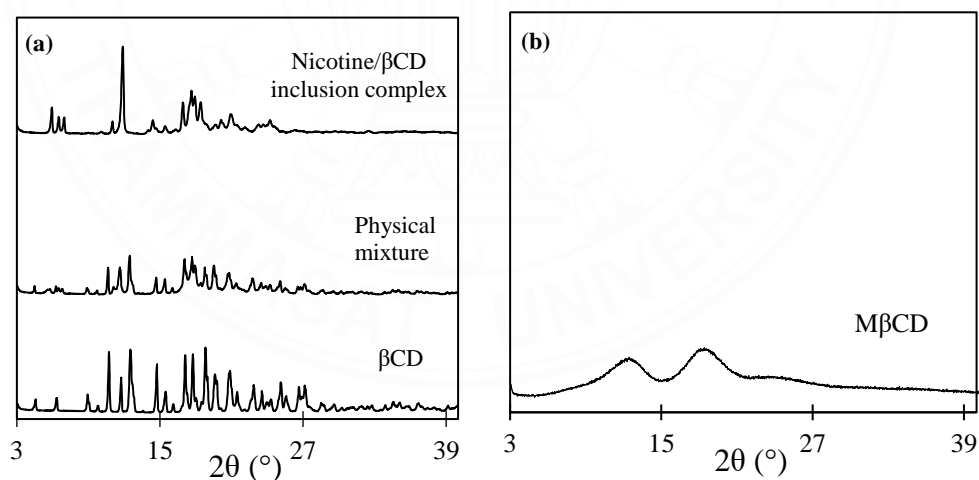
Figure 4.3 XRD patterns of (a) βCD, physical mixture, and nicotine/βCD inclusion complex and (b) MβCD

4.1.4.2 Fourier transform infrared (FTIR)

Figure 4.4(a) and (b) illustrate the FTIR spectra of inclusion complexes, βCD, MβCD, and pure nicotine. The characteristic peaks of each sample were summarized in Table 4.4.
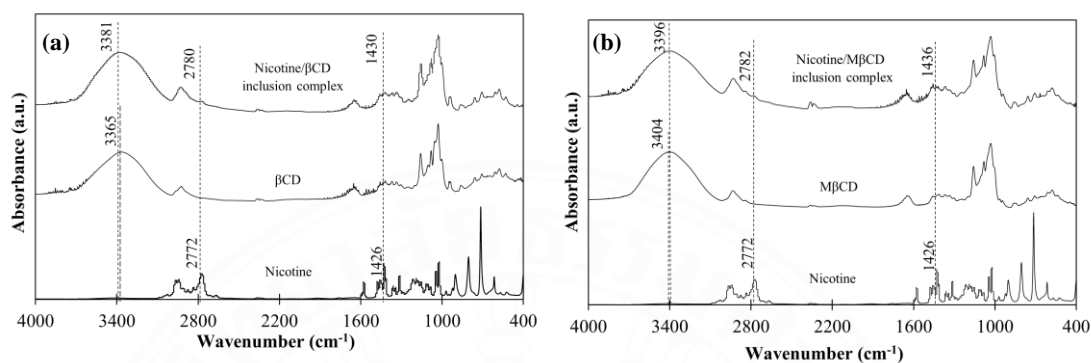
Figure 4.4 FTIR spectra of (a) inclusion complex, βCD, and nicotine (b) inclusion complex, MβCD, and nicotine

Table 4.4 Summary of functional groups of pure nicotine, βCD, and MβCD

Compound	Wavenumber (cm^{-1})	Vibrational mode
βCD	3365	O-H stretching
MβCD	3404	O-H stretching
Nicotine	2272	N-CH$_3$ stretching
	1426	C-N stretching

There are subtle peak shifts for nicotine/βCD and nicotine/MβCD inclusion complexes which confirm the complexes formation. According to Figure 4.4 (a) and (b), three main peak shifts which corresponds to O-H stretching, N-CH$_3$ stretching, and C-N stretching are observed. O-H stretching peaks are shifted to 3381 and 3396 cm^{-1}; N-CH$_3$ stretching peaks are shifted to 2780 and 2782 cm^{-1}; and C-N stretching peaks are shifted to 1430 and 1436 cm^{-1} for βCD and MβCD inclusion complexes, respectively. The FTIR results reveal that nicotine/βCD and nicotine/MβCD inclusion complexes generated different interactions when compared to the pure compounds which confirm the inclusion complexes formation.

4.1.4.3 Differential scanning calorimeter (DSC)
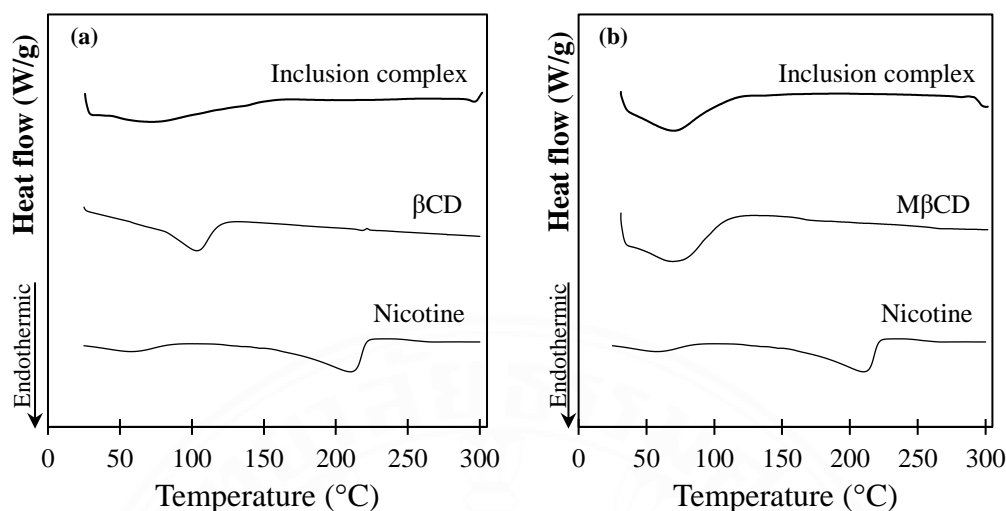
Figure 4.5 DSC curves of (a) nicotine, βCD, and nicotine/βCD inclusion complex and (b) nicotine, MβCD, and nicotine/MβCD inclusion complex

Figure 4.5(a) shows the DSC curves of the nicotine/βCD inclusion complex comparing to pure βCD and nicotine. Nicotine shows two endothermic peaks between 25 to 70 °C which is corresponding to the loss of moisture content due to its hygroscopic nature and between 150 to 220 °C which is corresponding to the volatilization of the compound. βCD shows a broad endothermic peak from 30 to 120 °C from the loss of moisture content. Nicotine/βCD inclusion complex also shows a broad endothermic peak from 30 to 150 °C from the loss of moisture content. There is no peak corresponding to the loss of nicotine from volatilization in the complex's curve. Therefore, the results imply the stabilized nicotine in form of the nicotine/βCD inclusion complex. Figure 4.5(b) shows the DSC curves of the nicotine/MβCD inclusion complex comparing to pure MβCD and nicotine. MβCD shows a broad endothermic peak from 30 to 120 °C from the loss of moisture content. Nicotine/MβCD inclusion complex shows a broad endothermic peak from 30 to 150 °C from the loss of moisture content. There is no peak corresponding to the loss of nicotine from volatilization which also implies the stabilized nicotine in form of the nicotine/MβCD inclusion complex.

## 4.1.4.4 Thermogravimetric analysis (TGA)
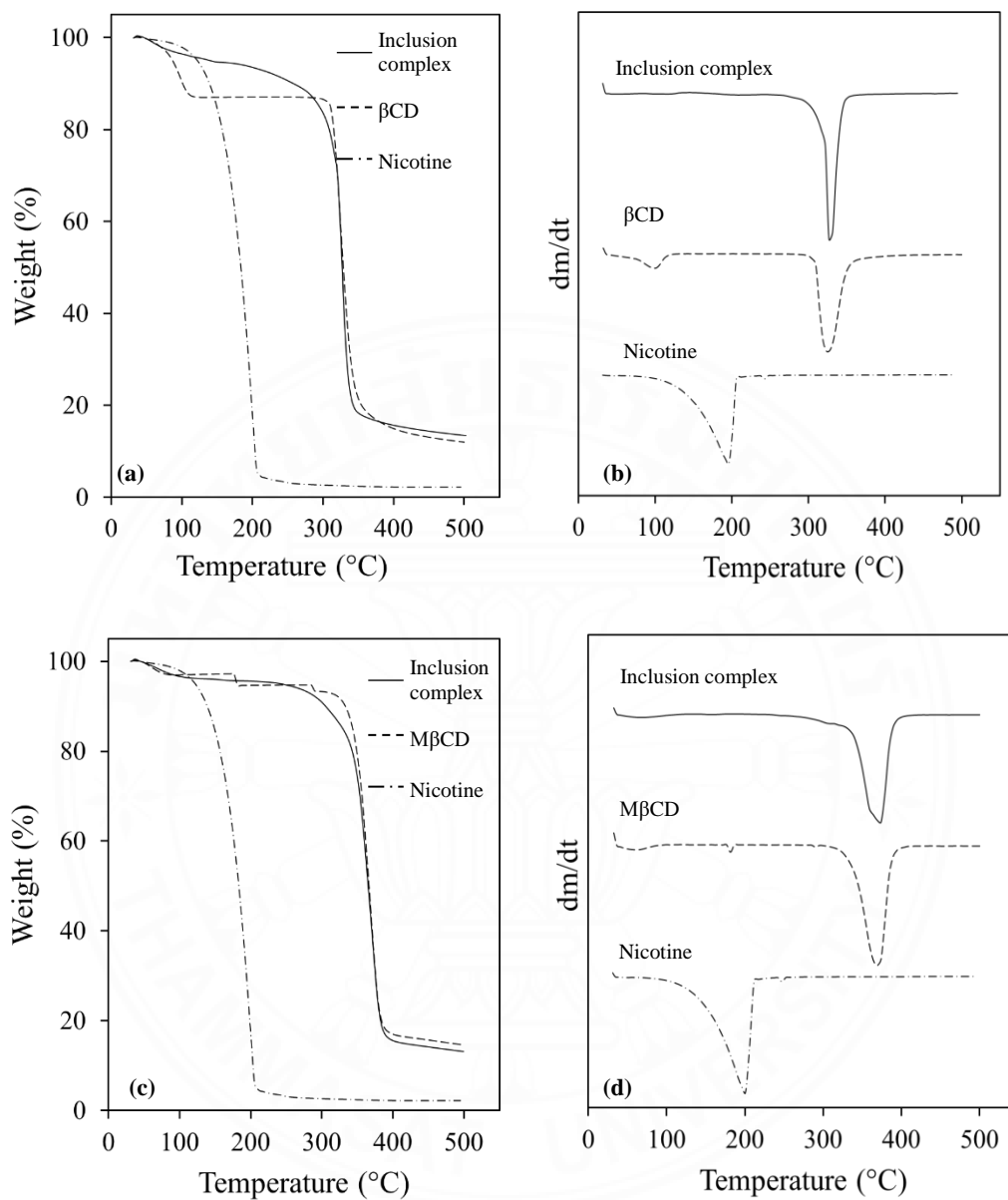
Figure 4.6 TG and DTG curves of (a) and (b) nicotine, βCD, and nicotine/βCD inclusion complex and (c) and (d) nicotine, MβCD, and nicotine/MβCD inclusion complex

Figure 4.6(a) to (d) illustrate the TG and DTG curves of the inclusion complex, βCD, MβCD, and nicotine, respectively. The TG profile of nicotine in free form shows the weight loss started in the range between room temperature and 230 °C from the volatilization. The TG profiles of βCD and MβCD show two-step weight loss which is from the loss of moisture content from 30 to 100 °C and the thermal decomposition temperature at 320 °C. The TG profiles of nicotine/βCD and nicotine/MβCD inclusion complex show the loss of moisture content and thermal decomposition of cyclodextrins without volatilization of nicotine. In conclusion, the improved thermostability of nicotine after encapsulation confirms the inclusion complex formation between nicotine and the cyclodextrins. Characterization results from FTIR, DSC, and TGA confirm the formation of nicotine/βCD and nicotine/MβCD inclusion complexes in the experimental study.
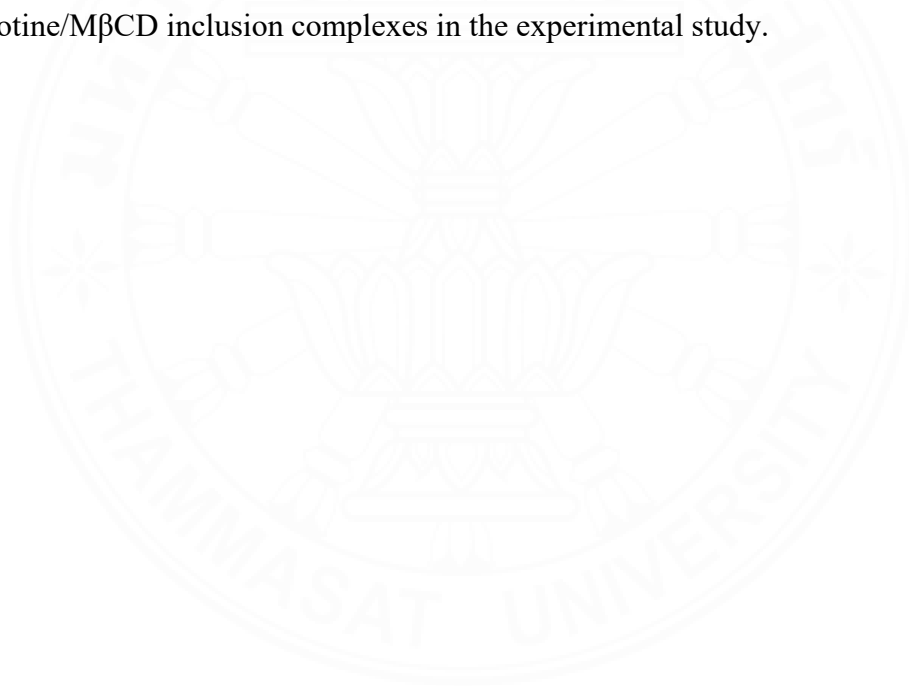
4.1.5 Evaluation of nicotine preservation

The nicotine/βCD inclusion complex and nicotine/MβCD inclusion complex were exposed to air at the storage temperature of 25 °C and 40 °C for 21 days to evaluate the preservation efficiency compared to pure nicotine.
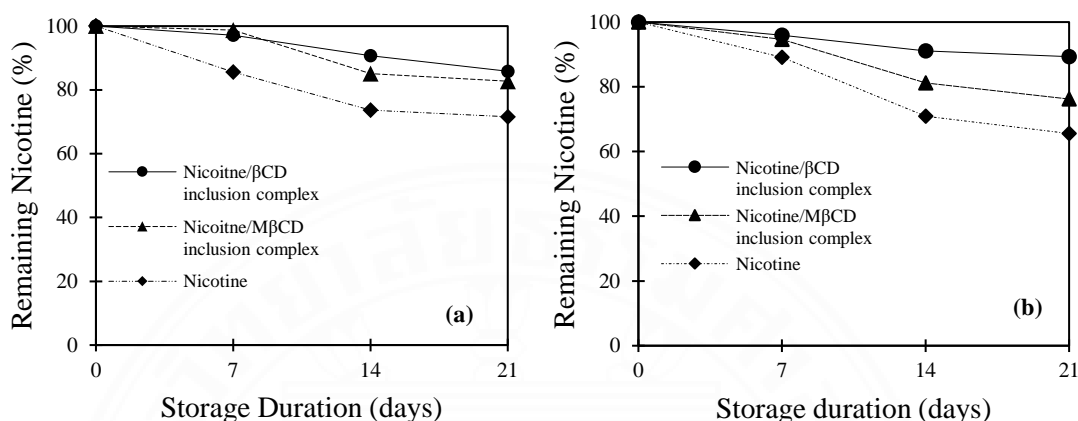
Figure 4.7 Evaluation of solanesol preservation at (a) 25 °C and (b) 40 °C

Figure 4.7(a) and (b) show the results of both form inclusion complex and pure nicotine, the remaining nicotine from pure nicotine after 21 days was 51.20% while the remaining nicotine from nicotine/βCD and nicotine/MβCD inclusion complexes were 84.83% and 81.97%, respectively. Furthermore, at 40 °C, the remaining nicotine from pure nicotine after 21 days was 50.34% while the remaining nicotine from nicotine/βCD and nicotine/MβCD inclusion complexes were 64.57% and 55.34%, respectively. Moreover, at 40 °C, amount of remaining nicotine from nicotine/MβCD inclusion complex is lower than nicotine/βCD inclusion complex. Since the vapor pressure at 40 °C is higher than 25 °C, the moisture content in air is higher which leads to the dissolution of MβCD due to its high water solubility. The releasing of nicotine from nicotine/MβCD inclusion complex results in the decreasing of remaining nicotine. However, the encapsulation of nicotine by both βCD and MβCD increases the amount of remaining nicotine. Therefore, βCD and MβCD can be used to preserve nicotine in the form of inclusion complexes.

4.1.6 Nicotine inclusion complex permeation though pig skin

Table 4.5 Amount of permeated nicotine toward pig skin in different forms

Sample	Amount of nicotine (μg)	
	30 min	60 min
Nicotine/βCD gel	4.08 ± 0.63	13.57 ± 0.18
Nicotine/MβCD gel	3.82 ± 0.67	9.81 ± 0.11
Nicotine gel	0.42 ± 0.02	0.95 ± 0.03

Table 4.5 shows the amount of permeated nicotine toward pig skin in different form. The amount of permeated nicotine was determined in two periods of time which are 30 min and 60 min. After 30 min, amount of permeated nicotine from both nicotine/βCD and nicotine/MβCD inclusion complex gels is 9 times as much as pure nicotine gel. Moreover, at 60 min, the amount of permeated nicotine from nicotine/βCD and nicotine/MβCD inclusion complex gels are 14 and 10 times as much as pure nicotine gel, respectively. Considering only inclusion complex gels, nicotine from nicotine/βCD inclusion complex has higher ability to permeate than that from nicotine/MβCD inclusion complex.

From the comparison of skin permeation results with the preservation study, the amount of permeated nicotine is limited by the stability of nicotine. Since nicotine in the form of inclusion complexes are more stable, the amount of permeated nicotine is higher than nicotine from pure nicotine gel. Moreover, between two types of inclusion complex gel, nicotine from nicotine/βCD inclusion complex permeates more than from nicotine/MβCD inclusion complex. Hence, the skin permeation study concludes that the amount of permeated nicotine depends on the stability which is the amount of remaining nicotine in the gel after a period of time.

4.2 Solanesol inclusion complex

4.2.1 Effect of ethanol on inclusion complex preparation

Table 4.6 shows encapsulation efficiency of solanesol inclusion complexes at various concentrations of ethanol (0-90 vol%). Result shows the increment of ethanol increased the encapsulation efficiency until saturated ethanol concentration at 70 vol%. The solvent effect study concluded that ethanol, co-solvent for preparation, not only improved the solubility of βCD but also increased the encapsulation efficiency of solanesol/CDs inclusion complex. However, ethanol increases the encapsulation efficiency until 70 vol% of ethanol-water solution after that the efficiency was reduced. Therefore, the concentration of ethanol for preparing solanesol/CDs inclusion complexes in this study was 70 vol%.

Table 4.6 Encapsulation efficiency of solanesol

Inclusion complex	Concentration of ethanol (vol%)	Encapsulation efficiency (%)
Solanesol /βCD	0	61.92 ± 2.18
	30	77.64 ± 3.61
	50	81.79 ± 0.99
	70	85.37 ± 3.10
	90	77.49 ± 7.03
Solanesol/MβCD	0	64.62 ± 5.57
	30	74.91 ± 3.34
	50	83.55 ± 7.71
	70	94.48 ± 2.67
	90	93.19 ± 7.66

4.2.3 Characterization

4.2.3.1 X-ray diffractometry (XRD)
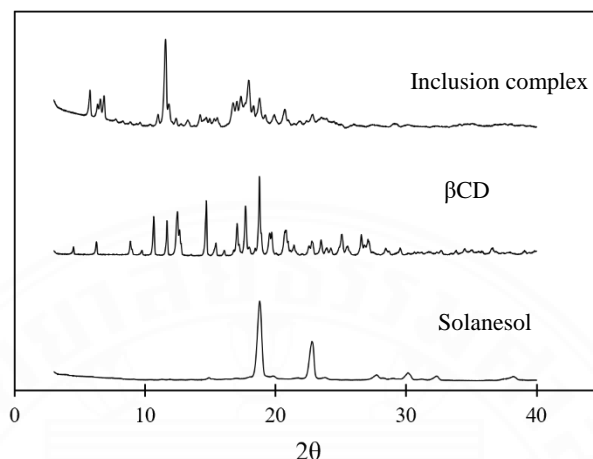
Figure 4.8 XRD pattern of solanesol, βCD, and solanesol/ βCD inclusion complex

Figure 4.8 illustrates the crystalline patterns of solanesol, βCD, and solanesol/βCD inclusion complex. The characteristic peaks of solanesol are at 18.69° and 22.68° (2θ). Characteristic peaks of βCD are at 10.73°, 12.43°, 15.39°,19.47°, 20.81°, and 22.73° (2θ). The XRD pattern of solanesol/βCD inclusion complex indicates the inclusion complex formation between solanesol and βCD due to the different patterns from pure solanesol and βCD. However, solanesol/MβCD cannot be characterized by XRD due to amorphous crystalline pattern of MβCD.

4.2.3.2 Fourier transform infrared (FTIR)

Figure 4.9(a) and (b) illustrates the FTIR spectra of inclusion complexes, βCD, MβCD, and pure solanesol. The characteristic peaks of each sample were summarized in Table 4.7.
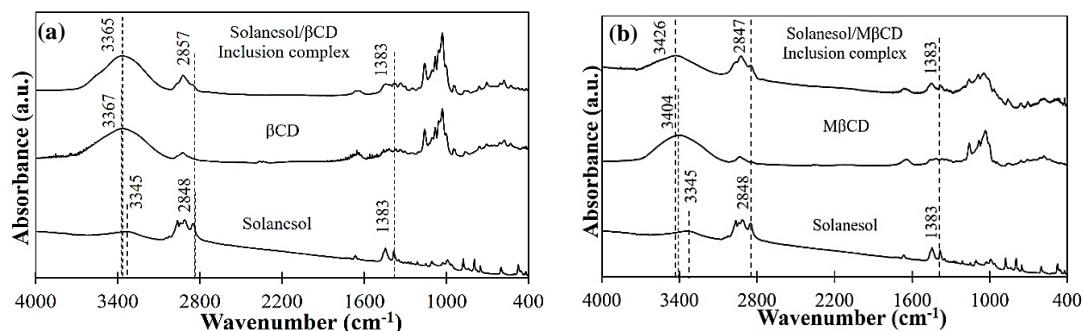
Figure 4.9 FTIR spectrogram of solanesol, (a) βCD, and solanesol/ βCD inclusion complex and (b)MβCD, and solanesol/MβCD inclusion complex

Table 4.7 Summary of functional groups in solanesol, βCD, and MβCD

Compound	Wavenumber (cm^{-1})	Vibrational mode
βCD	3367	O-H stretching
MβCD	3404	O-H stretching
Solanesol	3345	O-H stretching
	2848	C-H stretching
	1383	C-O stretching

There are subtle peak shifts for solanesol/βCD and solanesol/MβCD inclusion complexes which confirm the formation complexes. According to Figure 4.9(a) and (b), three main peaks are observed in solanesol/βCD and solanesol/MβCD inclusion complexes corresponds to O-H stretching, C-H stretching, and C-O stretching. O-H stretching peaks are at 3365 and 3426 cm^{-1}; C-H stretching peaks are at 2857 and 2847 cm^{-1}; and C-N stretching peaks are at 1383 cm^{-1} for βCD and MβCD inclusion complexes, respectively. The FTIR results imply that solanesol can form inclusion complexes with both βCD and MβCD.

4.2.3.3 Differential scanning calorimeter (DSC)
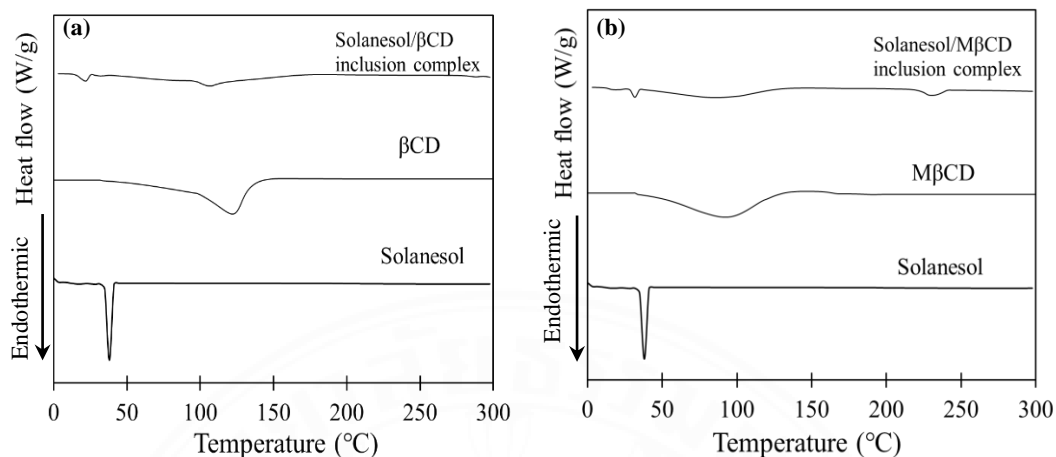
Figure 4.10 DSC curves of (a) solanesol, βCD, and solanesol/βCD inclusion complex
and (b) MβCD and solanesol/MβCD inclusion complex.

Figure 4.10(a) and (b) illustrate the DSC curves of solanesol, βCD, MβCD, and inclusion complexes. DSC curves of βCD and MβCD show a broad endothermic peak from 30 to 120 °C from the loss of moisture content. DSC curve of solanesol shows only one endothermic at 45 °C which is corresponding to melting point of solanesol. Both curves of solanesol in the form of inclusion complex show no endothermic peak corresponding to the melting of solanesol. The results imply that solanesol can form an inclusion complex with both βCD and MβCD with higher thermostability when compared to pure solanesol.

4.2.3.4 Thermogravimetric analysis (TGA)

Figure 4.11(a) to (d) illustrate the TG and DTG curves of the inclusion complex, βCD, MβCD, and solanesol, respectively.
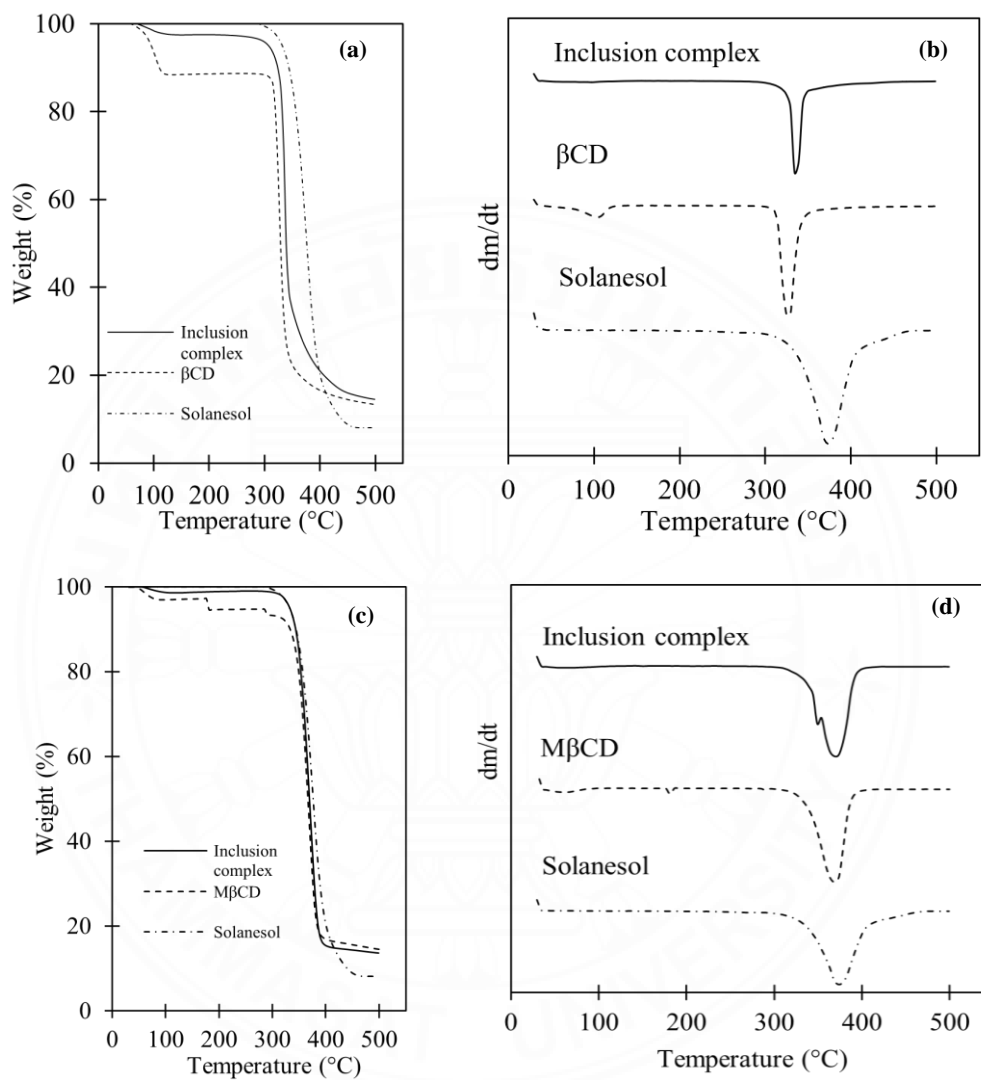

Figure 4.11 TGA and DTG curves of (a) and (b) solanesol, βCD, and solanesol/βCD inclusion complex and (c) and (d) solanesol, MβCD, and solanesol/MβCD inclusion complex

The TG profile of solanesol in the free form shows the weight loss started in the range between 350 °C and 450 °C from the thermal degradation. The TG and DTG profiles of βCD show two-step weight loss which is from the loss of moisture content from 30 to 150 °C and the thermal decomposition temperature at 320 °C. The TG and DTG profiles of the solanesol/βCD inclusion complex show only thermal decomposition of βCD without thermal degradation of solanesol. The improvement of thermostability confirms the inclusion complex formation between solanesol and βCD. Therefore, characterization results from FTIR, XRD, DSC, and TGA confirm the formation of solanesol/βCD inclusion complex.

The TG and DTG profiles of pure MβCD show the thermal degradation between 350 °C and 450 °C which is almost the same as pure solanesol. Therefore, the weight loss of solanesol/MβCD inclusion complex from the TG and DTG profiles appeared at the same temperature as both 2 pure compounds. The TGA results of solanesol/MβCD inclusion complex cannot be used to confirm the inclusion complex formation. Nevertheless, the other characterization methods including FTIR and DSC can verify the inclusion complex formation between solanesol and MβCD.

4.2.4 Evaluation of solanesol preservation
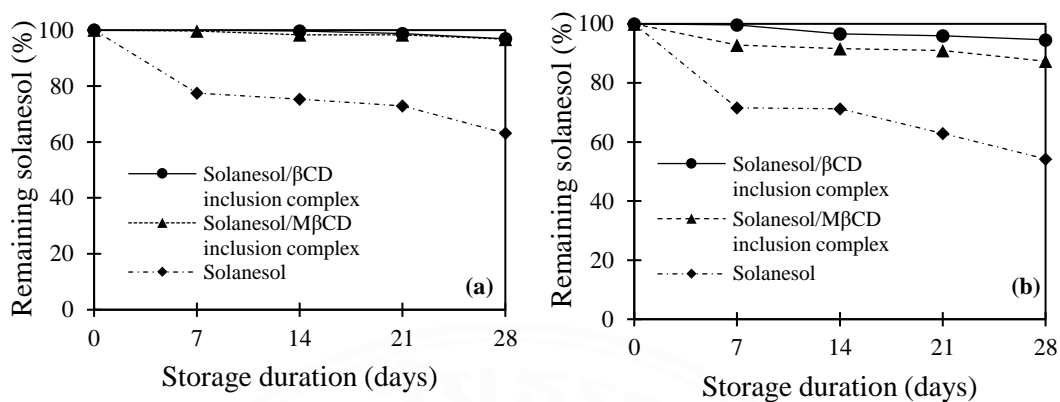
Figure 4.12 Evaluation of solanesol preservation at (a) 25 °C and (b) 40 °C

Figure 4.12(a) and (b) show the results of both form inclusion complex and solanesol. At 25 °C after 28 days, the remaining solanesol from pure solanesol was 63.12% while the remaining solanesol from solanesol/βCD and solanesol/MβCD inclusion complexes were 96.91% and 96.77%, respectively. Furthermore, at 40 °C, the remaining solanesol from pure solanesol after 28 days was 54.27% while the remaining solanesol from solanesol/βCD and solanesol/MβCD inclusion complexes were 94.60% and 87.34%, respectively. Moreover, at 40 °C, amount of remaining solanesol from solanesol/MβCD inclusion complex is lower than solanesol/βCD inclusion complex. Since the vapor pressure at 40 °C is higher than 25 °C, the moisture content in air is higher which leads to the dissolution of MβCD due to its high water solubility. The releasing of solanesol from solanesol/MβCD inclusion complex results in the decreasing of remaining solanesol. However, the encapsulation of solanesol by both βCD and MβCD increases the amount of remaining solanesol. Therefore, βCD and MβCD can be used to preserve solanesol in the form of inclusion complexes.

CHAPTER 5
CONCLUSION

This study investigated the preservation of two active compounds, nicotine and solanesol, by nanoencapsulation using βCD and MβCD. For nicotine, the computational simulation study shows the possible conformations of nicotine/βCD and nicotine/MβCD inclusion complexes with a host-guest molar ratio of 1:1. From the experimental study, the inclusion complexes were prepared with the same host-guest ratio as the results from the computational simulation. The XRD, FTIR, DSC, and TGA results confirm the inclusion complex formation between nicotine and both CDs. The preservation studies of nicotine in the form of inclusion complexes were performed under the storage temperature of 25 °C and 40 °C for 21 days. The results show the enhancement of nicotine stability after encapsulated by both βCD and MβCD when compared to pure nicotine. The remaining nicotine from nicotine/βCD inclusion complex is higher under both temperatures. Hence, βCD is more effective to stabilize nicotine. Moreover, the skin permeation study shows that the amount of permeated nicotine depends on its stability. Nicotine/βCD inclusion complex provides the highest permeated nicotine through pig skin. Thus, βCD can be used to enhance the skin permeation of nicotine for further use in the pharmaceutical industry.

Solanesol encapsulation technique using βCD and MβCD was investigated at 2:1 host-guest molar ratio as the computational simulation suggested. The XRD, FTIR, DSC, and TGA results confirm the inclusion complex formation between solanesol and both CDs. The preservation study of solanesol/CDs inclusion complex compared to pure solanesol shows the stability improvement of solanesol after encapsulated by CDs. Both βCD and MβCD are able to stabilize solanesol in the form of inclusion complexes. At the higher storage temperature (40 °C), βCD is more effective to stabilize solanesol.

Therefore, βCD and MβCD can form the inclusion complex with both active compounds, nicotine and solanesol, at the suggested host-guest molar ratio from the computational simulation. The nanoencapsulation technique can be applied to preserve both active compounds to prolong the shelf life in various applications.

REFERENCES

Armitage, A., Dixon, M., Frost, B., Mariner, D., & Sinclair, N. (2004). The effect of inhalation volume and breath-hold duration on the retention of nicotine and solanesol in the human respiratory tract and on subsequent plasma nicotine concentrations during cigarette smoking. *Beiträge zur Tabakforschung International/Contributions to Tobacco Research, 21*(4), 240-249.

Astray, G., Gonzalez-Barreiro, C., Mejuto, J. C., Rial-Otero, R., & Simal-Gandara, J. (2009). A review on the use of cyclodextrins in foods. *Food Hydrocolloids, 23*(7), 1631-1640.

Atla, S., Raja, B., & Dontamsetti, B. R. (2014). A New Method of Extraction, Isolation and Determination of Solanesol from Tobacco Waste (Nicotiana Tobacum L.) by Non-aqueous RP-HPLC. *Int. J. Pharm. Pharm. Sci, 6*, 543-546.

Balandrin, M. F., Klocke, J. A., Wurtele, E. S., & Bollinger, W. H. (1985). Natural plant chemicals: sources of industrial and medicinal materials. *Science, 228*(4704), 1154-1160.

Biovia, D. S. (2017). Discovery studio visualizer. *San Diego, CA, USA, 936*.

Coimbra, M., Isacchi, B., van Bloois, L., Torano, J. S., Ket, A., Wu, X., . . . Storm, G. (2011). Improving solubility and chemical stability of natural compounds for medicinal use by incorporation into liposomes. *International journal of pharmaceutics, 416*(2), 433-442.

Cui, H., Yurteri, C. U., Cabot, R., Xie, F., & Liu, H. (2019). Characterization of mainstream cigarette smoke aerosol by size-fractionated chemical analysis of nicotine, solanesol, and tobacco-specific nitrosamines. *Particulate Science Technology*, 1-9.

de Ong, E. (1924). Toxicity of Nicotine as an Insecticide and Parasticide. *Industrial Engineering Chemistry, 16*(12), 1275-1277.

Del Valle, E. M. (2004). Cyclodextrins and their uses: a review. *Process Biochemistry, 39*(9), 1033-1046.

Ezhilarasi, P., Karthik, P., Chhanwal, N., & Anandharamakrishnan, C. (2013). Nanoencapsulation techniques for food bioactive components: a review. *Food Bioprocess Technology, 6*(3), 628-647.

Ezhilarasi, P., Karthik, P., Chhanwal, N., Anandharamakrishnan, C. J. F., & Technology, B. (2013). Nanoencapsulation techniques for food bioactive components: a review. *6*(3), 628-647.

Flink, J. J. F. T. (1977). Energy analysis in [food] dehydration processes.

Frisch, M. J., Trucks, G. W., Schlegel, H. B., Scuseria, G. E., Robb, M. A., Cheeseman, J. R., . . . Fox, D. J. (2016). Gaussian 16 Rev. C.01. Wallingford, CT.

Gorrod, J. W., & Jacob III, P. (1999). *Analytical determination of nicotine and related compounds and their metabolites*: Elsevier.

Hadaruga, D. I., Hadaruga, N. G., Butnaru, G., Tatu, C., & Gruia, A. (2010). Bioactive microparticles (10): thermal and oxidative stability of nicotine and its complex with b-cyclodextrin. *J. Incl. Phenom. Macrocycl. Chem, 68*, 155-164.

Hedges, A. R. (1998). Industrial applications of cyclodextrins. *Chemical reviews, 98*(5), 2035-2044.

Hirayama, F., & Uekama, K. (1999). Cyclodextrin-based controlled drug release system. *Advanced drug delivery reviews, 36*(1), 125-141.

Hu, R.-S., Wang, J., Li, H., Ni, H., Chen, Y.-F., Zhang, Y.-W., . . . Li, H.-H. (2015a). Simultaneous extraction of nicotine and solanesol from waste tobacco materials by the column chromatographic extraction method and their separation and purification. *Separation Purification Technology, 146*, 1-7.

Hu, R.-S., Wang, J., Li, H., Ni, H., Chen, Y.-F., Zhang, Y.-W., . . . Li, H.-H. (2015b). Simultaneous extraction of nicotine and solanesol from waste tobacco materials by the column chromatographic extraction method and their separation and purification. *Separation Purification Technology, 146*, 1-7.

Huang, W., Li, Z., Niu, H., Wang, J., & Qin, Y. (2008). Bioactivity of solanesol extracted from tobacco leaves with carbon dioxide–ethanol fluids. *Biochemical engineering journal, 42*(1), 92-96.

Hudsin, N. D., G. scott. (2015). CDC – NIOSH Pocket Guide to Chemical Hazards – Nicotine.

Jadhav, R. P., Kengar, M. D., Nikam, N. R., & Bhutkar, M. A. (2019). Tobacco Cancer: A Review. *Asian Journal of Research in Pharmaceutical Science, 9*(4), 276-281.

Jiang, Z., Tang, G., & Lu, L. (2008). catena-Poly [[diiodidomercury (II)]-µ-nicotine-κ2N: N′]. *Acta Crystallographica Section E: Structure Reports Online, 64*(8), m1026-m1026.

Jin, Z.-Y. (2013). *Cyclodextrin chemistry: Preparation and application*: World Scientific.

Jokić, S., Gagić, T., Knez, Ž., Banožić, M., & Škerget, M. (2019). Separation of active compounds from tobacco waste using subcritical water extraction. *The Journal of Supercritical Fluids, 153*, 104593.

KLEPTOSE®, R. n. d. Betacyclodextrin. Retrieved from https://www.roquette.com/pharma-kleptose

Krake, A. M. (1999). Nicotine Fumigation: A Greenhouse Application. *Applied occupational environmental hygiene 14*(6), 349-355.

Linde, G. A., Laverde, A., & Colauto, N. B. (2011). Changes to taste perception in the food industry: use of cyclodextrins. In *Handbook of Behavior, Food and Nutrition* (pp. 99-118): Springer.

Liu XP, C. X., Li L, Wang XR, Li XC. (2007). Determination of solanesol in different parts of tobacco leaves from different breeds and planting areas by high performance liquid chromatography–mass spectrometry. *Roc Min Ana*, 26:105–108.

Manunza, B., Deiana, S., Pintore, M., & Gessa, C. (1997). Structure and internal motion of solvated beta-cyclodextrine: a molecular dynamics study. *Journal of Molecular Structure: THEOCHEM, 419*(1-3), 133-137.

McIndoo, N. (1916). Effects of nicotine as an insecticide. *Jour. Agr. Research, 7*(3), 89-122.

MI, H. W. H. (2005). Extraction and separation of solanesol from Nicotiana tobacum by supercritical fluid extraction and silica gel column chromatography. *Chinese Traditional and Herbal Drugs 36*, 690-692.

Morris, G. M., Huey, R., Lindstrom, W., Sanner, M. F., Belew, R. K., Goodsell, D. S., & Olson, A. J. (2009). AutoDock4 and AutoDockTools4: Automated docking with selective receptor flexibility. *Journal of computational chemistry, 30*(16), 2785-2791.

Ng, L.-K., & Hupé, M. (2003). Effects of moisture content in cigar tobacco on nicotine extraction: Similarity between Soxhlet and focused open-vessel microwave-assisted techniques. *Journal of Chromatography A, 1011*(1-2), 213-219.

Pinho, E., Grootveld, M., Soares, G., & Henriques, M. (2014). Cyclodextrins as encapsulation agents for plant bioactive compounds. *Carbohydrate polymers, 101*, 121-135.

Ruiz-Rodriguez, A., Bronze, M.-R., & da Ponte, M. N. (2008). Supercritical fluid extraction of tobacco leaves: A preliminary study on the extraction of solanesol. *The Journal of Supercritical Fluids, 45*(2), 171-176.

Santos, P. S., Souza, L. K., Araujo, T. S., Medeiros, J. V. R., Nunes, S. C., Carvalho, R. A., . . . Figueiras, A. (2017). Methyl-β-cyclodextrin Inclusion Complex with β-Caryophyllene: Preparation, Characterization, and Improvement of Pharmacological Activities. *ACS omega, 2*(12), 9080-9094.

Singh, R., Bharti, N., Madan, J., & Hiremath, S. (2010). Characterization of cyclodextrin inclusion complexes—a review. *J. Pharm. Sci. Technol, 2*(3), 171-183.

Sridevi, P., Vijayanand, P., & Raju, M. B. (2017). Formulation and evaluation of anti-inflammatory herbal gel containing isolated solanesol. *Ann. Phytomed, 6*, 127-131.

Sridevi, P., Vijayanand, P., & Raju, M. B. J. A. P. (2017). Formulation and evaluation of anti-inflammatory herbal gel containing isolated solanesol. *6*, 127-131.

Steiner, T., & Koellner, G. (1994). Crystalline. Beta.-cyclodextrin hydrate at various humidities: fast, continuous, and reversible dehydration studied by X-ray diffraction. *Journal of the American Chemical Society, 116*(12), 5122-5128.

Sun, Y.-h., Huang, R.-l., Xing, X.-x., Qi, W., Su, R.-x., & He, Z.-m. (2013). Enhanced extraction of solanesol from tobacco leaves by a new ammonia leaching pretreatment method. *Fine Chem, 30*, 32-35.

Szejtli, J. (2004). Past, present and futute of cyclodextrin research. *Pure Applied Chemistry, 76*(10), 1825-1845.

Szente, L., & Szejtli, J. (1999). Highly soluble cyclodextrin derivatives: chemistry, properties, and trends in development. *Advanced Drug Delivery Reviews, 36*(1), 17-28.

Tang, D.-S., Zhang, L., Chen, H.-L., Liang, Y.-R., Lu, J.-L., Liang, H.-L., & Zheng, X.-Q. (2007). Extraction and purification of solanesol from tobacco:(I). Extraction and silica gel column chromatography separation of solanesol. *Separation Purification Technology, 56*(3), 291-295.

Tayoub, G., Sulaiman, H., & Alorfi, M. (2015). Determination of nicotine levels in the leaves of some Nicotiana tabacum varieties cultivated in Syria. *Herba Polonica, 61*(4), 23-30.

Tucker, S. P., & Pretty, J. R. (2005). Identification of oxidation products of solanesol produced during air sampling for tobacco smoke by electrospray mass spectrometry and HPLC. *Analyst, 130*(10), 1414-1424.

Veer, V., & Gopalakrishnan, R. (2016). *Herbal insecticides, repellents and biomedicines: effectiveness and commercialization*: Springer.

Wada, E., Kisaki, T., & Saito, K. (1959). Autoxidation of nicotine. *Archives of Biochemistry Biophysics, 79*, 124-130.

Wang, Y., & Gu, W. (2018). Study on supercritical fluid extraction of solanesol from industrial tobacco waste. *The Journal of Supercritical Fluids, 138*, 228-237.

Xiang, D., Yao, Z., Liu, Y., Gai, X., Du, Y., Zhang, Z., . . . Fu, Q. (2017). Analysis on solanesol content and genetic diversity of Chinese flue-cured tobacco (Nicotiana tabacum L.). *Crop Science, 57*(2), 847-855.

Xiao Keyi, D. Y., Shi Wanqi, Li Jianzhong, Li Ying, Yin Shufan. (2012). Synthesis and Antitumor Activities of the Diacid Solanesyl 5-Fluorouracil Esters Derivatives. *32*(01), 169-173. doi:10.6023/cjoc1107042

Yan, N., Du, Y., Zhang, H., Zhang, Z., Liu, X., Shi, J., & Liu, Y. (2018). RNA sequencing provides insights into the regulation of solanesol biosynthesis in Nicotiana tabacum induced by moderately high temperature. *Biomolecules, 8*(4), 165.

Yan, N., Liu, Y., Gong, D., Du, Y., Zhang, H., & Zhang, Z. (2015). Solanesol: A review of its resources, derivatives, bioactivities, medicinal applications, and biosynthesis. *Phytochemistry Reviews, 14*(3), 403-417.

Yan, N., Liu, Y., Liu, L., Du, Y., Liu, X., Zhang, H., & Zhang, Z. J. B. (2019). Bioactivities and Medicinal Value of Solanesol and Its Accumulation, Extraction Technology, and Determination Methods. *9*(8), 334.

Zhang, Z.-s., & Feng, X. (2007). Study on ultrasonic assisted extraction of solanesol from tobacco leaves. *J. Food Sci. Biotechnol, 26*, 51-53.

ZHAO, C.-j., YANG, L., ZU, Y.-g., XIA, L.-h., & XIAO, C.-w. (2007). Extraction of solanesol by dynamic saponification method [J]. *Chemical Engineering, 9*.

APPENDICES

APPENDIX A
EXTRACTION, PURIFICATION AND CHARACTERIZATION
OF NICOTINE

Hu, R. et al. studied about factors that can be affected amount of nicotine by using solvation techniques. There are 3 factors that varied which are ratio of solvent, dissolving time, and effects from additional of NaOH added to ethanolic portion. Solvents that used in extraction are petroleum ether, ethanol, and mixture between petroleum ether and ethanol. The dissolution time and minimum solvent used was determined to be 4 h and 2 time of dried tobacco waste (v/w), i.e., 1 g of dried tobacco waste can absorb 2 mL of solvent at maximum as shown in Figure A.1. Moreover, another studied reported that nicotine is in form of bound or ester within the tobacco leaves. Therefore, alkali or acid added can be used to increase the extraction yield. The ratio between petroleum ether and ethanol in optimal condition is 4:6 (v/v) and dissolution is 4 h with 2% NaOH in ethanolic portion.
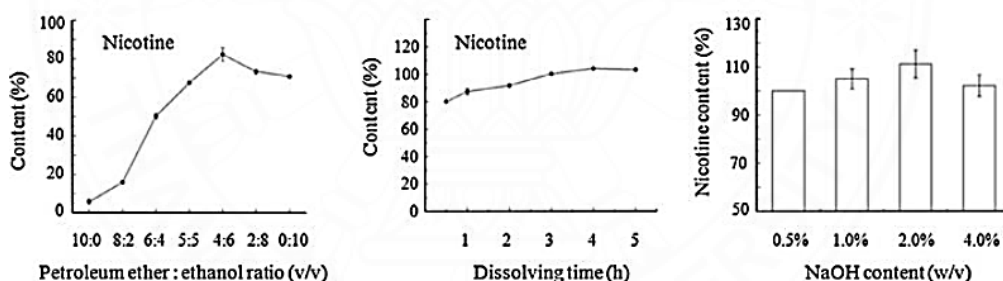

Figure A.1 Factors affected nicotine extraction: (a) effects from solvent (30 °C, 1 h, 20 rpm), (b) effects from dissolution time (30 °C, 20 rpm), and (c) effects from additional of NaOH added to ethanolic portion

After the extraction process, 1 mol of HCl was added into the solution for adjusting pH to be 2.0 and separating into 2 phases which are petroleum ether and ethanol aqueous phase. The 1/4 volume of 90% of acidic ethanol (pH 2.0) was used for washing petroleum ether phase and 1/4 volume petroleum ether was used for washing the ethanol phase. The vacuum-concentration of the ethanol aqueous phase was resulted in the nicotine aqueous solution. For purification process, the pH of nicotine aqueous solution was adjusted to be 10 and fractionated with petroleum ether for 3 times with equal volume (first time) and half volume (second and third time).

The combined petroleum ether phase was washed one time with 1/4 volume of alkaline water. The vacuum recovery of petroleum ether provided purified nicotine. After purification method, the nicotine purity was analyzed by using high performance liquid chromatography and the result was 99.30% (Hu et al., 2015b).
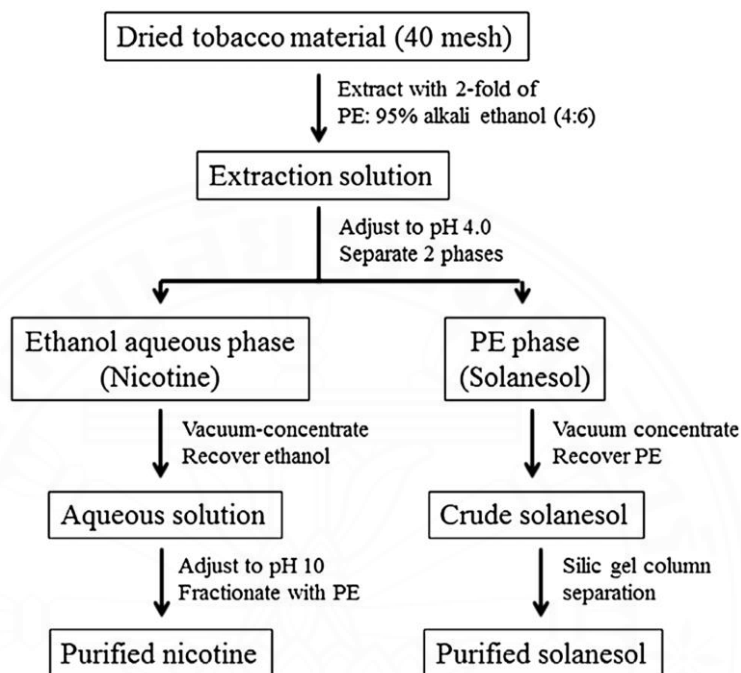

Figure A.2 Extraction and purification steps for nicotine and solanesol

Quantification conditions by using HPLC are provided. Chromatograms are shown in Figure D.3. Characterization of nicotine by HPLC was performed by using YMC packed ODS column (250 mm, 4.6 mm, 5 μm) with methanol and 0.2% triethylamine in aqueous solution (4:6 by volume) as mobile phase with flow rate of 0.8 mL/min and UV detector at the wavelength of 254 nm.
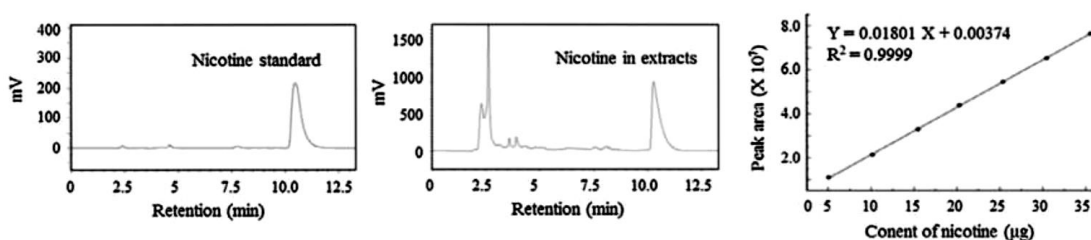

Figure A.3 HPLC chromatograms of nicotine and calibration curve

In another study, Ng, L., and Hupe, M. studied the extraction of nicotine by using Soxhlet extraction (Ng & Hupé, 2003). Soxhlet extraction (Figure A.4) is also popular method used to extract compound from plants. Burns and Collins describe the conditions for extracting nicotine as refluxing temperatures 99.2 and 64.5°C for isooctane and methanol (MeOH) solvent for 2 hours (Figure A.5).
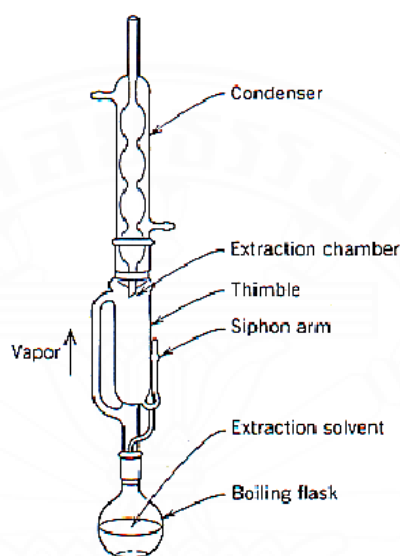

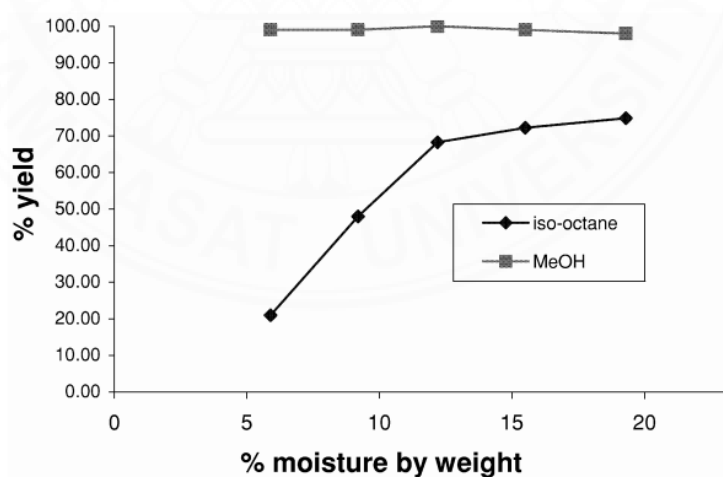**Figure A.4** Configuration of Soxhlet extractor (Source: www.researchgate.net)

Figure A.5 Moisture and solvent affected on nicotine content by

Soxhlet extraction (Ng & Hupé, 2003)

Methanol can effectively extract nicotine and has no effect by moisture content. However, extraction by using iso-octane is affected by moisture content. Low moisture content in tobacco leaves results in the shrinkage of cell membrane as shown in Figure A.5. Therefore, less iso-octane contacts with nicotine content inside cell membrane. For extra water content, the cell is more likely to rupture. While iso-octane is affected by moisture content, MeOH has its ability to permeate through cell wall. Thus, the effect of moisture content towards MeOH does not apply (Ng & Hupé, 2003).Characterization by using GC-FID is provided.

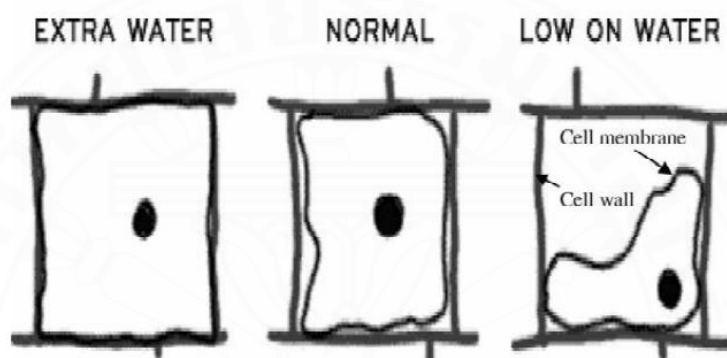**Figure A.6** Influence of moisture towards cell membrane in plant cell

Quantification conditions by using GC-FID was performed by using DB5MS column (30m×0.25 mm I.D 0.25 μm film). Helium flow was 1.0 mL/min. Oven temperature was maintained at 80°C for 1 min and ramped up to 30°C at 15°C/min and held for 1.5 min. Chromatograms are shown in Figure A.7 (Ng & Hupé, 2003).
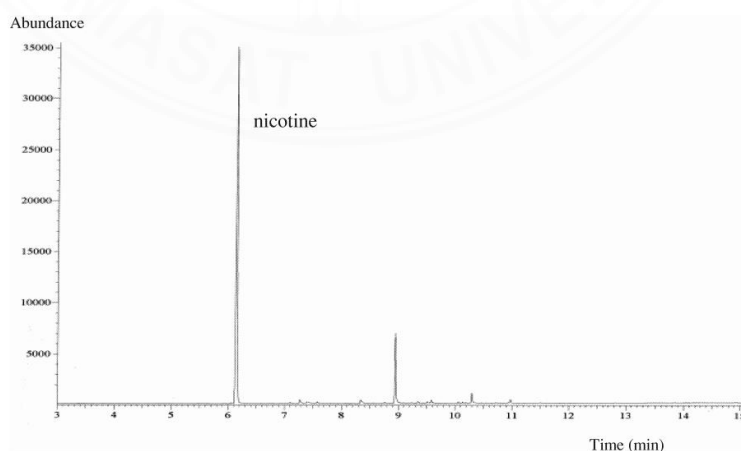
Figure A.7 GC-FID chromatogram of nicotine

FTIR spectra of nicotine can be assigned as 1677 (C=N stretching), 1691 (C=C aromatic stretching), 717 and 904 (out of plant C-H bending), and 1200–1350 cm^{-1} (C-N stretching) (Veer & Gopalakrishnan, 2016). The location of vibration is shown in Figure A.8.
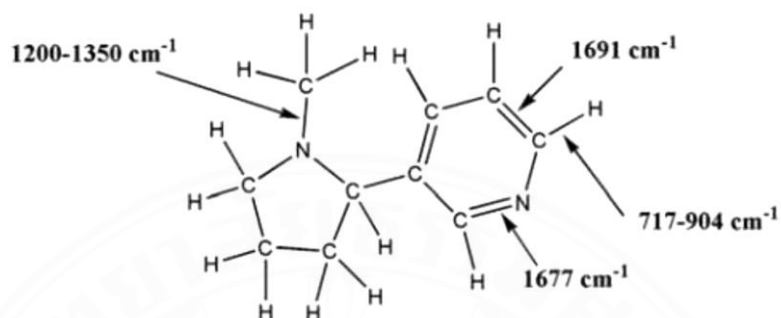

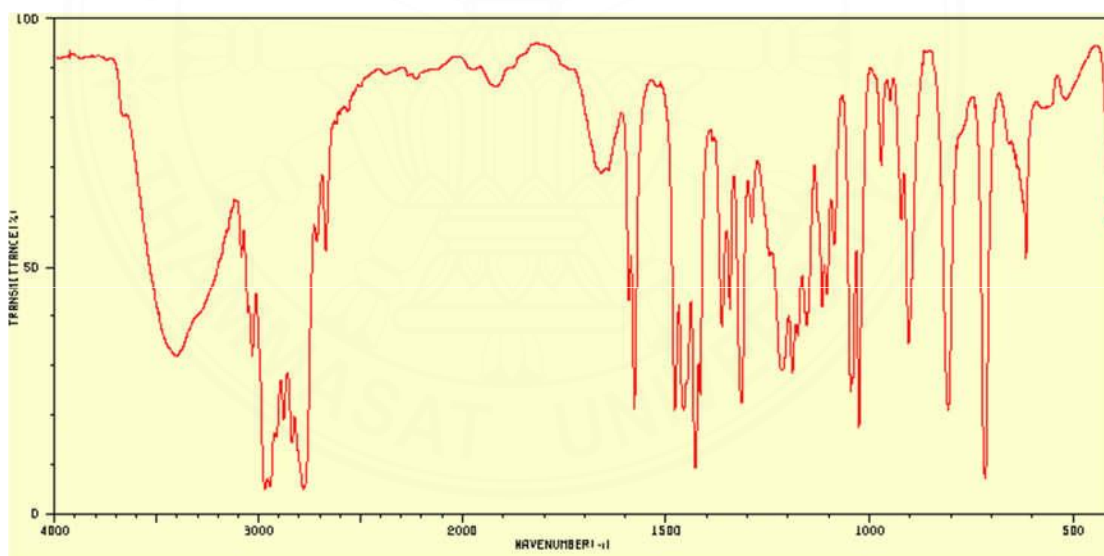**Figure A.8** FTIR band assignment on the structure of nicotine (Veer & Gopalakrishnan, 2016)

Figure A.9 FTIR spectra of nicotine

APPENDIX B
PURIFICATION AND CHARACTERIZATION OF SOLANESOL

As shown in Figure A.1, Hu, R. et al. also studied about purification of solanesol from extracted crude (Hu et al., 2015a). The crude solanesol was dissolved and loaded onto the column and eluted with 1,2-dichloroethane. The amounts of solanesol in purified product that can be determined by using HPLC was 93.1% and recovery rate is 87.4% in the column chromatographic step.

Quantification conditions by using HPLC are provided. Chromatograms are shown in Figure B.1. Characterization solanesol by HPLC was performed by using YMC packed ODS column (250 mm, 4.6 mm, 5 μm) with a Solanesol was analyzed by using 100% of methanol as a mobile phase, flow rate is 0.8 mL/min and detected by using UV detector at 215 nm.
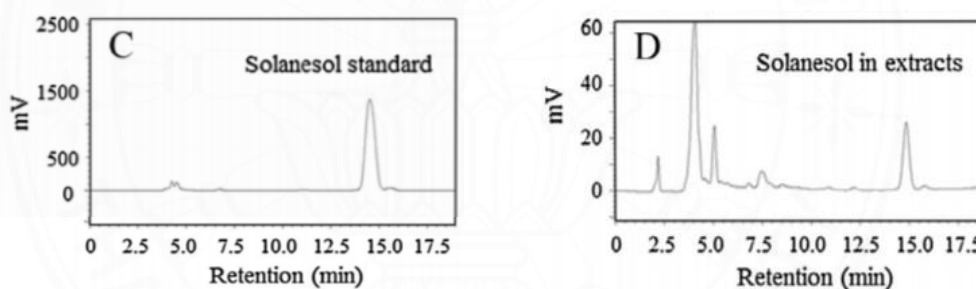

Figure B.1 HPLC chromatograms of solanesol

In another study, Srinivasa Rao Atla (Atla, Raja, & Dontamsetti, 2014) studied about solanesol extraction and determined amount of solanesol content in tobacco waste. Briefly extraction process is shown in Figure B.2. First, 25 kg of dried tobacco wastes were submerged in petroleum ether to make crude solanesol and rotary vacuum evaporator was used for concentrating the petroleum ether solution. Purification of crude extracted solanesol was performed by three different methods and compared the yield of products. Purified product by saponification followed by recrystallization with different solvents is the best which give yield is 0.05% and purity of solanesol is 92 %.
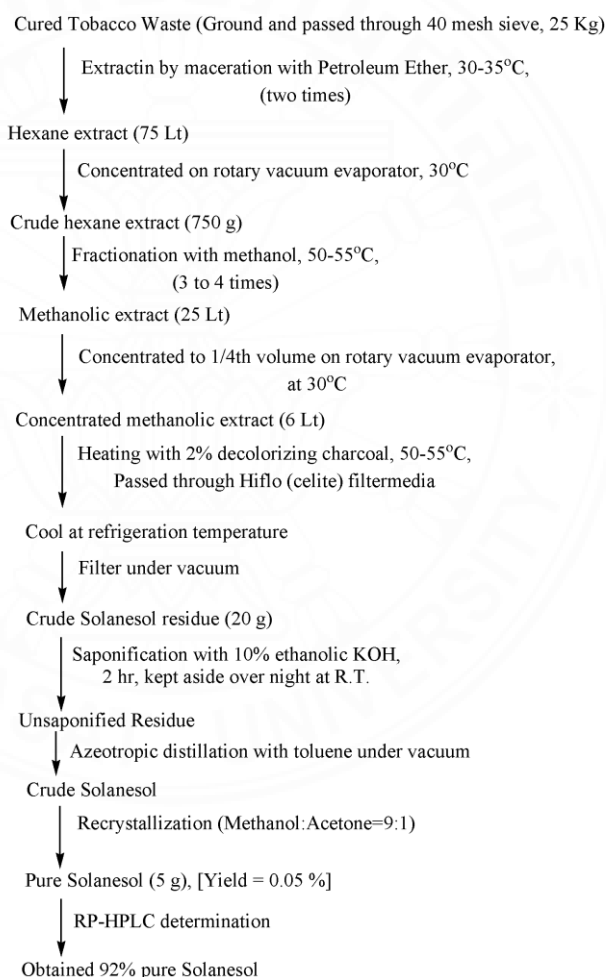
Cured Tobacco Waste (Ground and passed through 40 mesh sieve, 25 Kg)

Extractin by maceration with Petroleum Ether, 30-35°C,
(two times)

Hexane extract (75 Lt)

Concentrated on rotary vacuum evaporator, 30°C

Crude hexane extract (750 g)

Fractionation with methanol, 50-55°C,
(3 to 4 times)

Methanolic extract (25 Lt)

Concentrated to 1/4th volume on rotary vacuum evaporator,
at 30°C

Concentrated methanolic extract (6 Lt)

Heating with 2% decolorizing charcoal, 50-55°C,
Passed through Hiflo (celite) filtermedia

Cool at refrigeration temperature

Filter under vacuum

Crude Solanesol residue (20 g)

Saponification with 10% ethanolic KOH,
2 hr, kept aside over night at R.T.

Unsaponified Residue

Azeotropic distillation with toluene under vacuum

Crude Solanesol

Recrystallization (Methanol:Acetone=9:1)

Pure Solanesol (5 g), [Yield = 0.05 %]

RP-HPLC determination

Obtained 92% pure Solanesol

Figure B.2 Isolation and purification of solanesol from tobacco waste

Quantification conditions by using HPLC are provided. Chromatograms are shown in Figure B.3. Characterization of solanesol by HPLC was performed by using Phenomenex Luna C18 (250 mm, 4.6 mm i.d., particle size 5 μm). Methanol:IPA (60:40, v/v) was used as mobile phase at 1.0 mL/min flow rate, injection volume 10 μL, and detected (by UV) at 215 nm.
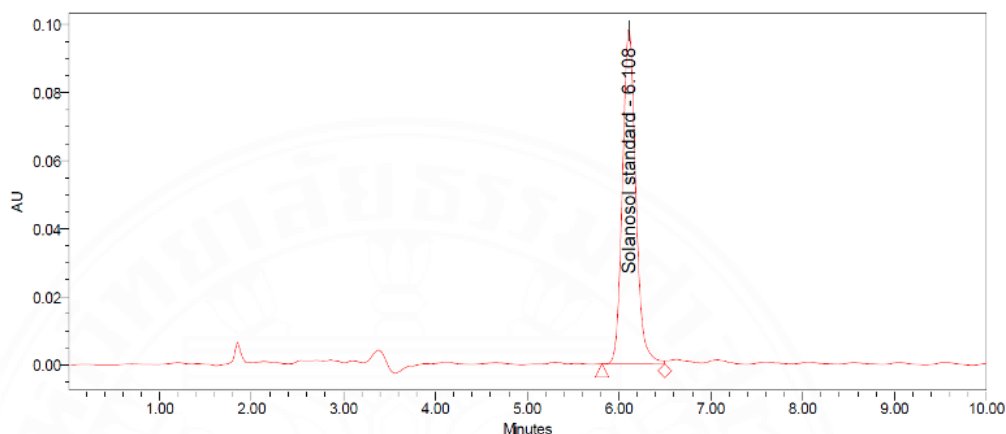

Figure B.3 HPLC Chromatogram of solanesol standard

The band assignment of solanesol determined by using Fourier Transform Infrared (FTIR) with KBr were listed in Table B.1.

Table B.1 FTIR band assignment of solanesol (P. Sridevi, P. Vijayanand, & M. B. J. A. P. Raju, 2017)

Functional groups	Wavelength (cm^{-1})
OH group	3,490
C-H	3,018
C=C	1,516
C-H bending	670
C-C stretching	1,433
C-O	1,215
=C-H bending	759

APPENDIX C

INFRARED SPECTRUM OF BCD AND MBCD

FTIR band assignments of βCD showed in Table C.1.

Table C.1 FTIR band assignment of βCD

Functional groups	Wavelength (cm^{-1})
OH stretching	3,467
C-H stretching	2,926
C-H bending	1,420
Coupled C-C-H, C-O-H, and H-C-H bending	1,337
Coupled C-O, C-C, and C-O-H vibration	1,166 and 1,094
Skeleton vibration at α-1,4 linkage	942

The subtle changes of βCD spectrum can be occurred after formation of inclusion complex. Patil Dipak, R., et al. studies the inclusion complex of parachlorobenzonitrile. They found that the shift of spectrum can be detected at –CH stretching (2,926 cm^{-1} for βCD and 2,924 cm^{-1} for inclusion complex) and broad –OH stretching peak (~3,400 cm^{-1}) for βCD comparing to sharp –OH peak for inclusion complex.
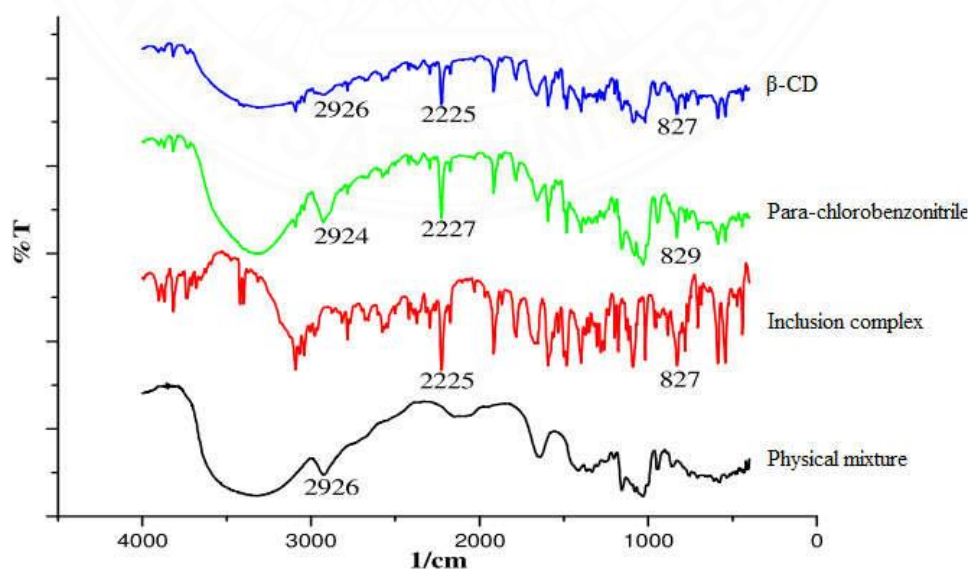

Figure C.1 FTIR spectrum and subtle changes due to complex formation

The band assignments of MβCD showed in Table C.2. Pauline S. Santos studied about inclusion complex between MβCD and essential oil (Santos et al., 2017). The FTIR spectrum of MβCD, physical mixture (PM), and inclusion complex in different methods showed in Figure C.2. For physical mixture, spectrum show the characteristic peak of essential oil at 886 cm^{-1} but it absents in inclusion complex spectrum due to complex formation.

Table C.2 Band assignments of MβCD

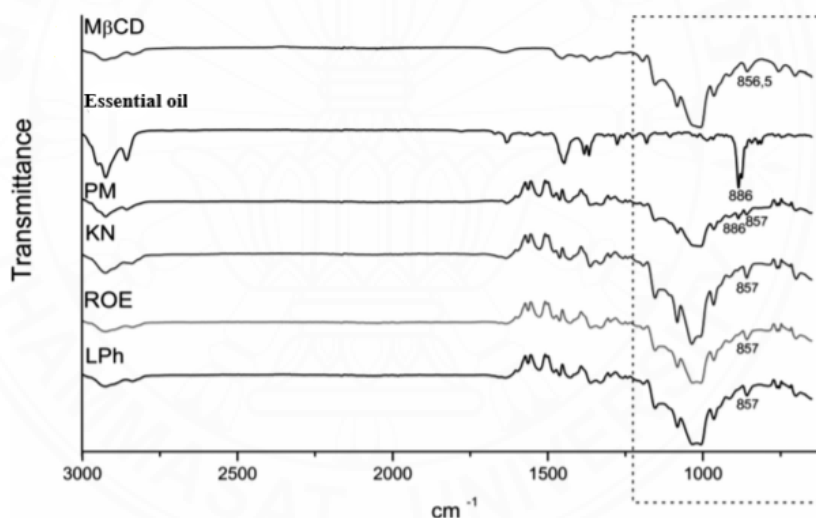| Functional groups	Wavenumber (cm^{-1})
O−H stretching	3,385
C−H stretching	2,928
C−O stretching compatible to the bonds on ether and hydroxyl groups	1,193, 1,082, and 1,022

Figure C.2 FTIR spectrum of essential oil, physical mixture, and inclusion complex in different methods

BIOGRAPHY

Name	Mr. Sorrawee Chulurks
Date of Birth	June 18, 1996
Education	2020: Bachelor of Engineering (Chemical Engineering)
	Sirindhorn International Institute of Technology
	Thammasat University

Publication

Chulurks, S., Toochinda, P., & Lawtrakul, L. (2021). Computational and Experimental Studies of Nicotine Inclusion Complex with β-cyclodextrin and Methylated-β-cyclodextrin. Proceedings of *the 30TH Institute of Chemical Engineering and Applied Chemistry Conference* (pp. 389-397). Thailand: School of Chemical Engineering, Institute of Engineering, Suranaree University of Technology.